Tectonophysics 776 (2020) 228321

Contents lists available at ScienceDirect

Tectonophysics

journal homepage: www.elsevier.com/locate/tecto

Love-to-Rayleigh scattering across the eastern North American passive margin

Andrea Servali[a], Maureen D. Long[a,*], Jeffrey Park[a], Margaret H. Benoit[b], John C. Aragon[a,c]

[a] Department of Geology and Geophysics, Yale University, PO Box 208109, New Haven, CT 06520, USA
[b] National Science Foundation, 2415 Eisenhower Ave., Alexandria, VA 22314, USA
[c] Now at Earthquake Science Center, U.S. Geological Survey, Menlo Park, CA 94025, USA

ARTICLE INFO

Keywords:
Seismic anisotropy
Surface waves
Wave scattering
Eastern North America
Mantle flow
Lithospheric deformation

ABSTRACT

This study presents observations of Love-to-Rayleigh scattering beneath the eastern North American passive margin that place new constraints on seismic anisotropy in the upper mantle. The scattering of Love-wave energy to Rayleigh waves is generated via sharp lateral gradients in anisotropic structure along the source-receiver path. The scattered phases, known as quasi-Love (QL) waves, exhibit amplitude behavior that depends on the strength of the anisotropic contrast as well as the geometrical relationship between the propagation azimuth and the anisotropic symmetry axis. Previous studies of seismic anisotropy in the upper mantle beneath eastern North America have revealed evidence for a mix of lithospheric and asthenospheric contributions, but the interpretation of indicators such as SKS splitting is hampered by a lack of vertical resolution. Complementary constraints on the depth distribution of anisotropy can be provided by surface waves, which have the additional advantage of sampling portions of the margin that lie offshore. Here we present measurements of QL phases using data from several hundred broadband seismic stations in eastern North America, including stations of the USArray Transportable Array, the Central and Eastern U.S. Network, and the MAGIC experiment in the central Appalachians. We find evidence for clear QL arrivals at stations in eastern North America, consistent with a region of particularly strong and coherent scattering inferred just offshore the central portion of the margin. The coherent scattering near the Eastern North American Margin likely reflects lateral transitions in seismic anisotropy in the asthenospheric mantle, associated with locally complex three-dimensional flow, with possible additional contributions from anisotropy in the mantle lithosphere. A second region of strong QL scattering near the southern coast of Greenland is enigmatic in origin, but may be due to pre-existing lithospheric fabric.

1. Introduction

The Eastern North American Margin (ENAM) is a mature passive continental margin that reflects a rich range of tectonic processes affecting its structure and evolution over the past billion years. These processes include the Grenville Orogeny (e.g., Rivers, 1997, 2009; Whitmeyer and Karlstrom, 2007; McLelland et al., 2010), which culminated in the formation of the Rodinia supercontinent roughly 1.1 Gyr ago, the rifting apart of Rodinia during the Cambrian (e.g., Li et al., 2008; Burton and Southworth, 2010), and the Paleozoic Appalachian Orogeny, which culminated in the formation of the Pangea supercontinent (e.g., Hatcher, 2010; Hibbard et al., 2010). The breakup of Pangea was accomplished via a complex set of rifting processes (e.g., Withjack et al., 2012; Frizon de Lamotte et al., 2015) that encompassed the emplacement of the Central Atlantic Magmatic Province (CAMP) (e.g., McHone, 1996, 2000; Schlische, 2003). Subsequent to rifting, the margin underwent nearly 200 Myr of modification, and there is ample evidence for ongoing lithospheric evolution and young dynamic processes in the mantle beneath ENAM (e.g., Miller et al., 2013; Mazza et al., 2014, 2017; Menke et al., 2016, 2018; Levin et al., 2018; Wagner et al., 2018; Byrnes et al., 2019; Evans et al., 2019).

It is generally understood that tectonic processes such as subduction and rifting modify the structure of the continental crust and mantle lithosphere (e.g., Gashawbeza et al., 2004; Zheng et al., 2012; Long et al., 2012; Eilon et al., 2014; Accardo et al., 2014; Eakin et al., 2014; Bishop et al., 2017; Garzione et al., 2017). However, the details of such lithospheric modification are not well understood; in particular, in regions that have undergone multiple episodes of major tectonism, it remains a challenge to identify and interpret the range of structures that may have resulted. Our ability to study the structure of the crust,

* Corresponding author.
E-mail address: maureen.long@yale.edu (M.D. Long).

https://doi.org/10.1016/j.tecto.2020.228321
Received 11 July 2019; Received in revised form 7 January 2020; Accepted 10 January 2020
Available online 15 January 2020
0040-1951/

mantle lithosphere, and asthenospheric mantle beneath ENAM has been hampered by the relatively sparse coverage of broadband seismic stations. This situation has recently improved dramatically, however, due to data collection initiatives that include the EarthScope USArray (www.usarray.org), the Central and Eastern U.S. Network (www.usarray.org/ceusn), and the GeoPRISMS ENAM Community Seismic Experiment (ENAM CSE; www.udc.ig.utexas.edu). These data present new opportunities to image the crust and mantle beneath ENAM in unprecedented detail and relate newly discovered structures to past tectonic events or to ongoing dynamic processes.

Seismic anisotropy, or the directional dependence of seismic wave speeds, is a particularly interesting property to study, because there is a relatively direct link between (past and present) deformation and the resulting anisotropy. This link arises when (crustal or mantle) rocks are deformed in the dislocation creep regime; their constituent minerals tend to align in preferred orientations, and this texture gives rise to macroscopic anisotropy (e.g., Karato et al., 2008; Skemer and Hansen, 2016). Seismic anisotropy can be interrogated using a variety of techniques, but the most commonly used is the measurement of shear wave splitting or birefringence (e.g., Silver, 1996; Savage, 1999; Long and Silver, 2009), often of core-refracted phases such as SKS. SKS splitting beneath ENAM was studied in the pre-USArray era (Barruol et al., 1997; Levin et al., 1999; Fouch et al., 2000; Long et al., 2010; Wagner et al., 2012). These studies revealed complex patterns in measured splitting parameters (fast splitting direction, ϕ, and delay time, δt). These early observations were thought to generally require contributions from anisotropy in both the lithosphere (reflecting frozen-in structure from past deformation events) and the asthenosphere (reflecting deformation due to present-day mantle flow), but the sparse station coverage hampered more detailed interpretations. Newer SKS splitting studies that take advantage of dense arrays in the ENAM region (Long et al., 2016; Yang et al., 2017; White-Gaynor and Nyblade, 2017; Aragon et al., 2017; Lynner and Bodmer, 2017; Chen et al., 2018; Levin et al., 2018) reveal rich and complex patterns in both ϕ and δt, but quantifying the relative contributions from the lithosphere and the asthenosphere remains a difficult problem.

Constraints on seismic anisotropy complementary to those provided by SKS splitting can be obtained by examining surface waves; because of their dispersive properties, surface waves, when observed at different periods, can shed light on the depth distribution of anisotropy. One strategy is to incorporate azimuthal anisotropy into surface-wave tomography models (e.g., Deschamps et al., 2008; Wagner et al., 2018), although anisotropy and isotropic wavespeed heterogeneity can trade off in such inversions, and some studies have struggled to reconcile surface wave and SKS splitting constraints on anisotropy (e.g., Wagner and Long, 2013; Wagner et al., 2018). Another strategy is to look for evidence for the scattering of Love-wave energy to Rayleigh-wave energy; such scattered waves are known as quasi-Love (QL) phases (e.g., Park and Yu, 1993; Oda and Onishi, 2001; Levin et al., 2007; Rieger and Park, 2010; Chen and Park, 2013; Margheriti et al., 2014). Love-to-Rayleigh scattering results from the coupling of toroidal and spheroidal modes in the presence of anisotropy, and is particularly sensitive to lateral gradients in anisotropy along the raypath.

In this study, we look for evidence of Love to Rayleigh scattering recorded at seismic stations in eastern North America, including those of the USArray Transportable Array (TA), the Central and Eastern U.S. Network, and the MAGIC Flexible Array experiment in the central Appalachians. Our goal is to obtain constraints on seismic anisotropy (and, in particular, its lateral variability and depth distribution) that are complementary to those provided by SKS splitting studies of the region. Analysis of QL phases has been successfully applied to USArray data in Cascadia (Rieger and Park, 2010), but has not yet been applied to data from ENAM. We implemented an objective algorithm for the identification of QL phases and measurement of their timing and amplitude. We identified coherent and relatively high-amplitude QL phases for several earthquakes, with clear geographic patterns. Our analysis revealed two areas of significant QL scattering, one located offshore North America and one near the southern coast of Greenland. We infer that QL scattering offshore from ENAM results from a sharp transition in upper mantle anisotropy across the margin, consistent with previous SKS studies. While the exact mechanism for the transitions in anisotropy suggested by our data cannot be uniquely determined, the QL observations documented in our study are numerous, robust, and yield consistent geographic patterns.

2. Data and methods

2.1. Quasi-Love waves as an indicator of anisotropic gradients

Quasi-Love (QL) waves result from the scattering of energy from Love waves (surface waves with horizontal motion perpendicular to the direction of wave propagation, arriving on transverse component seismograms) to Rayleigh waves (surface waves with both vertical and horizontal motion, arriving on the vertical and radial component seismograms). The QL waveforms are generally similar to those of the Love waves, but they propagate at Rayleigh-wave velocities. These QL arrivals are not expected for isotropic Earth models; rather, their generation requires a lateral gradient in upper mantle seismic anisotropy (Park and Yu, 1993), and results from the coupling of toroidal (Love) and spheroidal (Rayleigh) modes. While QL phases are a reliable indicator of sharp gradients in anisotropy, they can be somewhat challenging to observe, as their amplitude is typically small (~5–10% of the Love-wave amplitude for lateral anisotropic gradients of ~3–5%, as shown by Yu et al., 1995). Furthermore, the QL amplitude depends on the geometry of anisotropy, with maximum scattering when the (horizontal) symmetry axis of anisotropy is oriented 45° from the direction of wave propagation (Park, 1997).

Here we follow a similar observation strategy as previous studies of quasi-Love scattering (e.g., Park and Yu, 1993; Yu et al., 1995; Levin et al., 2007; Rieger and Park, 2010; Chen and Park, 2013) and identify the possible presence of a QL phase on the vertical component seismogram in the time window between the Love and Rayleigh arrivals. Because QL waves travel at Rayleigh-wave velocities, the scattered phase will arrive on the seismogram between the Love and Rayleigh waves. The difference in propagation velocity and the relative timing of the phases can be exploited to determine the location of the sharp anisotropic gradient responsible for the hybrid QL phase. Chen and Park (2013) carried out a back-projection of scattered QL phases along great-circle paths to estimate the locations of anisotropic scatterers, an approach that we follow in this study.

2.2. Data selection

We used data collected by an extensive set of broadband seismometers located in eastern North America, between 20°N and 60°N latitude and 67°W and 90°W longitude (Fig. 1). We included data from the USArray Transportable Array stations (network code TA), the Central and Eastern U.S. Network (N4), and the U.S. National Seismic Network (US). We also examined data from the temporary Mid-Atlantic Geophysical Integrative Collaboration, or MAGIC, experiment (network code 7A), a dense linear array deployed across the central Appalachians as part of the USArray Flexible Array between 2013 and 2016 (Aragon et al., 2017; Long et al., 2019; Byrnes et al., 2019; Evans et al., 2019). Taken together, we examined data from approximately 400 stations that cover the footprint of much of the Appalachians. We selected events for analysis from among shallow (hypocenter depths less than 100 km), large earthquakes occurring between 2011 and 2018. We initially examined earthquakes with moment magnitudes of 6.5 or greater, but found that only events of 7.0 or greater provided Love and Rayleigh arrivals that were robust enough to potentially observe scattered QL arrivals above the noise level. We initially considered events at epicentral distances between 20° and 120°, but found that only

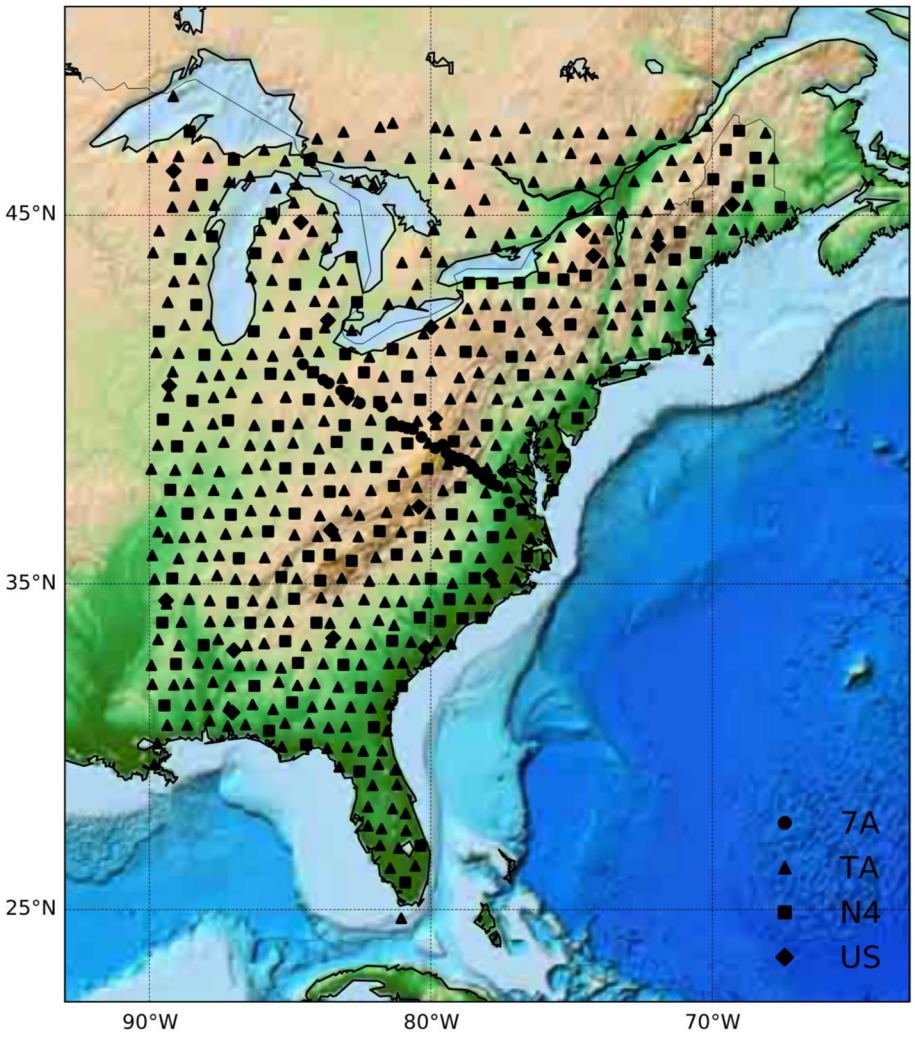

Fig. 1. Map of stations used in the analysis. USArray Transportable Array stations are indicated with triangles, Central and Eastern U.S. Network stations with squares, U.S. National Network stations with diamonds, and MAGIC stations with circles. Background colors indicate topography and bathymetry.

earthquakes at distances greater than 60° led to records with the required time separation between the main Love and Rayleigh arrivals needed to distinguish between the two phases and their respective wave trains. In all, we identified 12 events that were suitable for analysis (Fig. 2), with most earthquakes located either in the South American or Scotia subduction zones, along the southern portions of the Mid-Atlantic Ridge or East Pacific Rise, or in the area surrounding the Himalayas (including the magnitude 7.9 Gorkha earthquake in Nepal in April 2015).

2.3. Data preprocessing and measurement strategy

Our data preprocessing procedures closely followed those of previous studies, particularly Chen and Park (2013). We applied a series of identical low-pass filters (corner period of 100 s) to the data, finding that we obtained smooth waveforms after the sequential application of 3–4 filters. Because we applied the same sequence of filters to both the transverse and the vertical components, we expect that the relative time between the QL arrival and the main Rayleigh wave arrival was not strongly affected by the filtering process; see also Chen and Park (2013). In this study, we focus on measuring surface waves at periods of 100 s, because this is the period range at which QL phases are typically easiest to observe (e.g., Park and Yu, 1993; Levin et al., 2007; Rieger and Park, 2010; Chen and Park, 2013). However, measuring Love-to-Rayleigh scattering over a range of frequency bands is a natural target for future work. We next rotated the horizontal components to the great-circle path, to reveal Rayleigh waves on the radial (and vertical) component and Love waves on the transverse component. In order to robustly identify QL phases in the data, even in the presence of long-period noise and (possibly) multiple interfering scattered waveforms, we adopted a uniform, objective methodology for waveform processing.

Our first step was to compare the observed waveforms to synthetic seismograms generated for global upper mantle models that do not include sharp lateral gradients in azimuthal anisotropy, and therefore do not contain scattered QL phases. We obtained 3D synthetic seismograms generated using the spectral element method for each earthquake from the Princeton Shakemovie portal (Tromp et al., 2010). These synthetic ground displacement records were calculated using Global CMT Project focal mechanisms (Ekström et al., 2012) for a 3D Earth model (S362ANI) with radially anisotropic mantle structure (Kustowski et al., 2008) and crustal structure from the Crust2.0 model (Bassin et al., 2000). We processed the synthetic seismograms by convolving them with an appropriate source-time function (IRIS DMC, 2014) and applying a filtering routine identical to that applied to the actual data. We then removed the instrument response from the data to allow for a straightforward comparison between data and synthetics. We visually inspected the vertical component waveforms in the time window between the Love-wave arrival (identified on the transverse component) and the Rayleigh-wave arrival, to identify anomalous scattered arrivals in the data that did not appear in the synthetics. Our

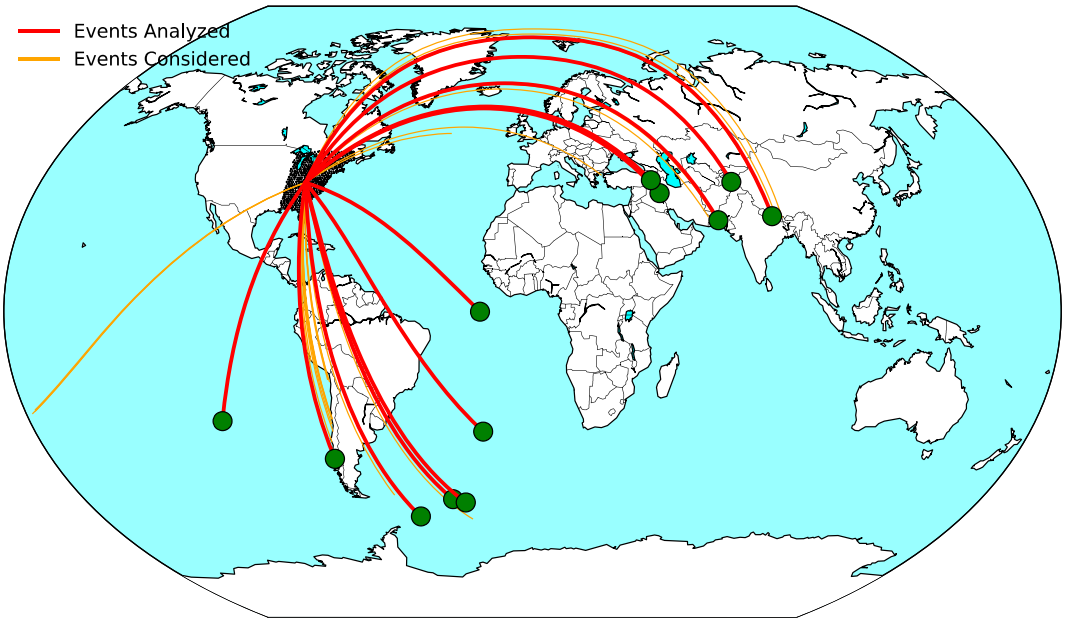

Fig. 2. Map of raypaths and earthquakes used in this study. Light orange lines indicate great-circle raypaths for events that were considered but not analyzed; dark red lines show great-circle paths for 12 events that were analyzed for QL arrivals, with green circles indicating the corresponding event locations. Great-circle raypaths were calculated for a representative station located in the center of the study area. (For interpretation of the references to color in this figure legend, the reader is referred to the web version of this article.)

analysis focused on identifying a single QL arrival in the time window between Love and Rayleigh wave arrivals, and so does not account for the possible presence of multiple QL arrivals. We also do not explicitly account for the possibility of multiple scattering; we assume single scattering when backprojecting the scattering points along the raypath, as discussed below. More than one scatterer could theoretically be present along the raypath; this would likely lead to error in our estimated location of a single scatterer. Waves that scatter more than once, however, are likely to have significantly lower amplitudes, and are thus unlikely to be a primary contributor to the waveforms under study.

Data traces that contained scattered energy on the vertical component were processed to measure the delay time between the Love and QL phases, as well as their amplitude ratios. Delay times were measured via cross-correlation in the time domain, and computed as the difference between the maximum autocorrelation of the Love-wave arrival (on the transverse component) and the maximum correlation of the transverse and vertical components (that is, the Love and QL arrivals). This analysis assumes that the scattered QL phase has a waveform shape similar to the parent Love waveform. We next tested the inferred QL waveforms for elliptical particle motion (as expected for a scattered Rayleigh wave) by examining the particle motion (in the radial plane; that is, the motion given by the radial and vertical components) in a 200 s window around the QL arrival. Candidate phases that did not display the expected elliptical particle motion were not characterized as QL arrivals.

The last analysis step was to measure the amplitude of the QL phase relative to that of the main Love-wave arrival. We measured this amplitude ratio, A, as:

$$A = \frac{\sqrt{\sum V(t)^2}}{\sqrt{\sum T(t)^2}} \quad (1)$$

where V(t) and T(t) are the vertical and transverse component time series, respectively. We summed the vertical component waveform over a 200 s window from the onset of the QL arrival (as measured by cross-correlation, as discussed above), while we summed the transverse component waveform over a flexibly defined window (typically around 400 s) that contains the main Love-wave arrival. While we did use a relatively long time window to compute the amplitude ratios, we did not expect any contribution from other phases in this window. This expectation was borne out by our comparison with the synthetic seismograms; additionally, all data were visually inspected to ensure that other phases were not obviously contaminating the amplitude measurements. Fig. 3 illustrates our QL measurement process for a single event observed at two nearby stations in the central Appalachians.

3. Results

3.1. Individual event results and examples

Each of the 12 events examined in this study (all of which exhibited significant Rayleigh and Love arrivals across the array; Table 1) exhibited at least some Love-to-Rayleigh scattering, observed as robust QL phase arrivals. Five events were located such that their raypaths arrived in eastern North America roughly from the north to northeast, while the remaining seven raypaths arrived from the south to southeast (Fig. 2 and Table 1). This raypath configuration gave us good coverage of the entire ENAM margin, including the region just offshore the coastline, as well as the southern portion of Greenland. We first discuss characteristics of the seismograms for individual events that indicate QL arrivals, and then discuss patterns of scattering for groups of events that indicate anisotropic gradients in particular regions in Section 3.2 below.

We begin by showing examples of particularly clear QL waveforms for two events, one located in the Scotia subduction zone (Fig. 4), and the other located in Nepal (Fig. 5). In the first example (Fig. 4, bottom panels), we show transverse and vertical component waveforms for stations located in and around the central Appalachians, including two stations of the MAGIC array (WINE and YLDA) and four surrounding TA stations. For each set of seismograms, the Love wave is clearly visible on the transverse component record, arriving at a time of roughly 4500–4600 s after the origin time (depending on distance). The Rayleigh wave is also clearly visible on the vertical component, although with lower amplitude and a more diffuse wave train, arriving 4800–4900 s after the origin time. Also on the vertical component, a clear QL arrival is visible at each station in the time window nearly coincident (or just after) the Love-wave arrival (red arrows in Fig. 4).

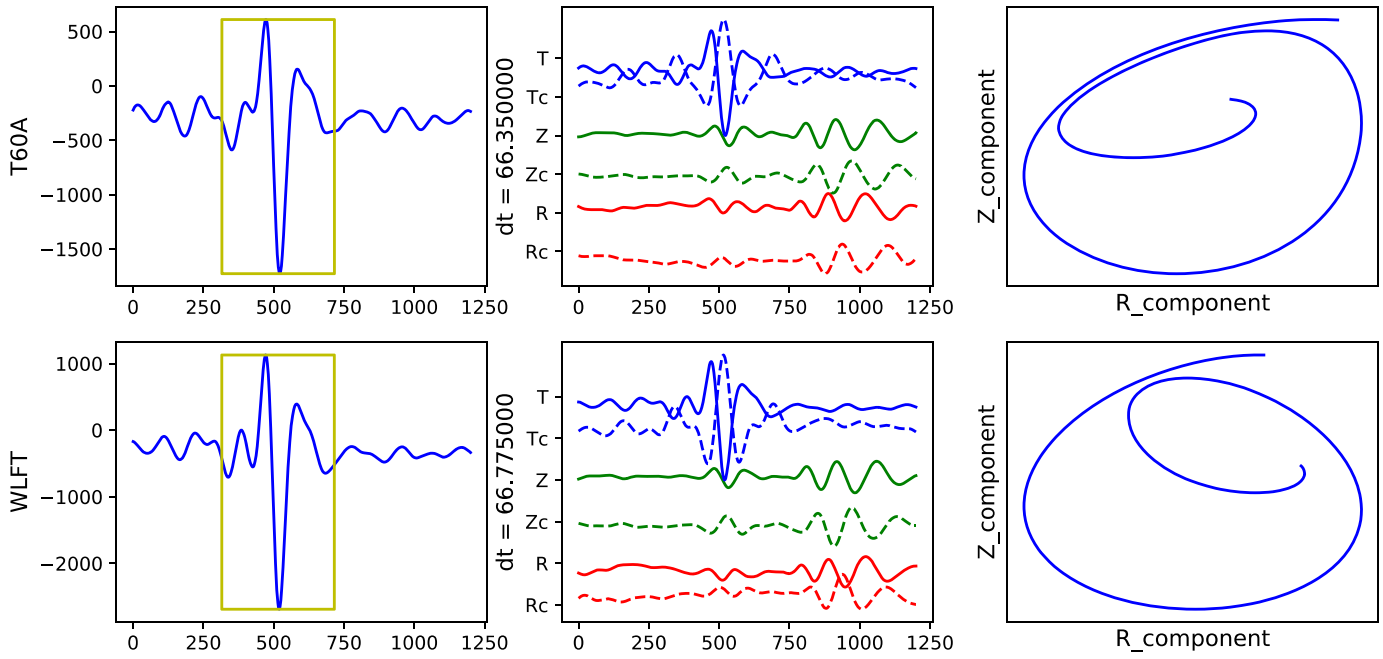

Fig. 3. Illustration of measurement procedure for a single event (magnitude 7.4, on August 19, 2016, located in the Scotia subduction zone) at two stations in the central Appalachian Mountains (TA station T60A, top row, and MAGIC station WLFT, bottom row). Left panels show transverse component waveforms (from an arbitrary time at $t = 0$), with the Love-wave arrival outlined by the yellow box. Center panels show, from top: transverse component waveform (solid blue line), autocorrelation of transverse component waveform (dashed blue line), vertical component waveform (solid green line), cross-correlation of transverse and vertical component waveform (dashed green line), radial component waveform (solid red line), and cross-correlation of transverse and radial component waveforms (dashed red line). The anomalous QL waveform is clearly visible on the vertical and radial components, close to the time window of the Love arrival. The measured delay times between the Love and QL arrivals are 66 s for station T60A and 67 s for station WLFT. Right panels show particle motion diagrams (in the radial plane) for the QL arrival, demonstrating elliptical particle motion. (For interpretation of the references to color in this figure legend, the reader is referred to the web version of this article.)

Table 1
Event information for earthquakes used in this study. Columns indicate the event date (YYYY.MM.DD), moment magnitude, latitude, longitude, and approximate backazimuth (calculated for a raypath measured in the central portion of our study area).

Event date	Magnitude	Latitude	Longitude	Backazimuth
2011.10.23	7.1	38.73°	43.45°	40°
2013.09.24	7.3	26.91°	65.53°	32°
2013.11.17	7.8	−60.38°	−46.59°	164°
2014.10.09	7.0	−32.30°	−110.92°	207°
2015.04.25	7.9	28.13°	84.72°	14°
2015.06.17	7.9	−35.37°	−17.81°	133°
2015.12.07	7.2	38.21°	72.78°	21°
2016.05.28	7.2	−56.24°	−26.94°	153°
2016.08.19	7.4	−55.28°	−31.87°	154°
2016.08.29	7.1	−0.05°	−31.87°	105°
2016.12.25	7.6	−43.41°	−73.94°	175°
2017.11.12	7.3	34.91°	45.96°	41°

The QL arrivals have similar wave shapes to the main Love arrivals and have amplitudes that are a relatively small fraction (14–28%, with some variability among stations) of the Love-wave amplitudes. Their timing, with arrivals generally within ~10 s of the Love-wave arrivals (as measured via cross-correlation), suggests that the scattering points are within a few hundred km of the stations. Following Chen and Park (2013), we back-project along the great-circle raypaths to estimate the location of the scatterers based on their timing (using nominal velocities for 100 s Rayleigh and Love waves in the upper mantle of 4.0 km/s and 4.4 km/s, respectively). These locations are shown in Fig. 4 (top panel), and point to a consistent region of scattering located just offshore from the ENAM coastline, at an approximate latitude of 35°.

In the second example (Fig. 5), we again observe consistent QL phase arrivals, but their timing is considerably different. Here we show data from the April 2015 Gorkha earthquake, recorded at a group of stations from the MAGIC experiment (WTMN, WINE, and RTSN) and from the TA. As with the earlier example, the transverse and vertical component waveforms show clear Love and Rayleigh arrivals, respectively (Fig. 5, bottom panels). In addition to the clear, high-amplitude Rayleigh waves, we also observe lower-amplitude arrivals between the Love and Rayleigh arrivals, which we interpret as QL phases (red arrows in Fig. 5). In contrast to the example shown in Fig. 4, these QL phases arrive considerably later than the Love waves (time delays of ~100 s), suggesting that the scattering points lie several thousand km away from the stations. Measured QL amplitudes range from ~10%–20% of the Love-wave amplitude, similar to the range observed for the previous example. When we backprojected along the great-circle raypaths, we found that the data suggest a coherent region of scattering beneath central Greenland (Fig. 5, top panel).

As discussed in Section 2.3, our identification of QL waves for each of the 12 events under study was informed by visual comparisons between actual data and synthetic seismograms generated for an Earth model without sharp lateral gradients in anisotropy (Tromp et al., 2010). We illustrate this comparison with an example, shown in Fig. 6, that shows observed and synthetic waveforms for an event on August 18, 2016, recorded at seven selected stations (including three from the MAGIC array) throughout our study region. These stations were selected because they each showed clear QL arrivals close in time to the main Love arrival. A comparison between the synthetic records (red traces) and the actual data (black traces) reveals that the synthetic seismograms generally match the observed Rayleigh and Love-wave arrivals, although there are modest differences between the observed and predicted waveforms (particularly in their amplitudes). Fig. 6 also shows a clear arrival on the vertical component of the actual data, coincident (or nearly so) with the Love-wave arrival on the transverse component, that is not visible on the synthetic waveforms. (We note

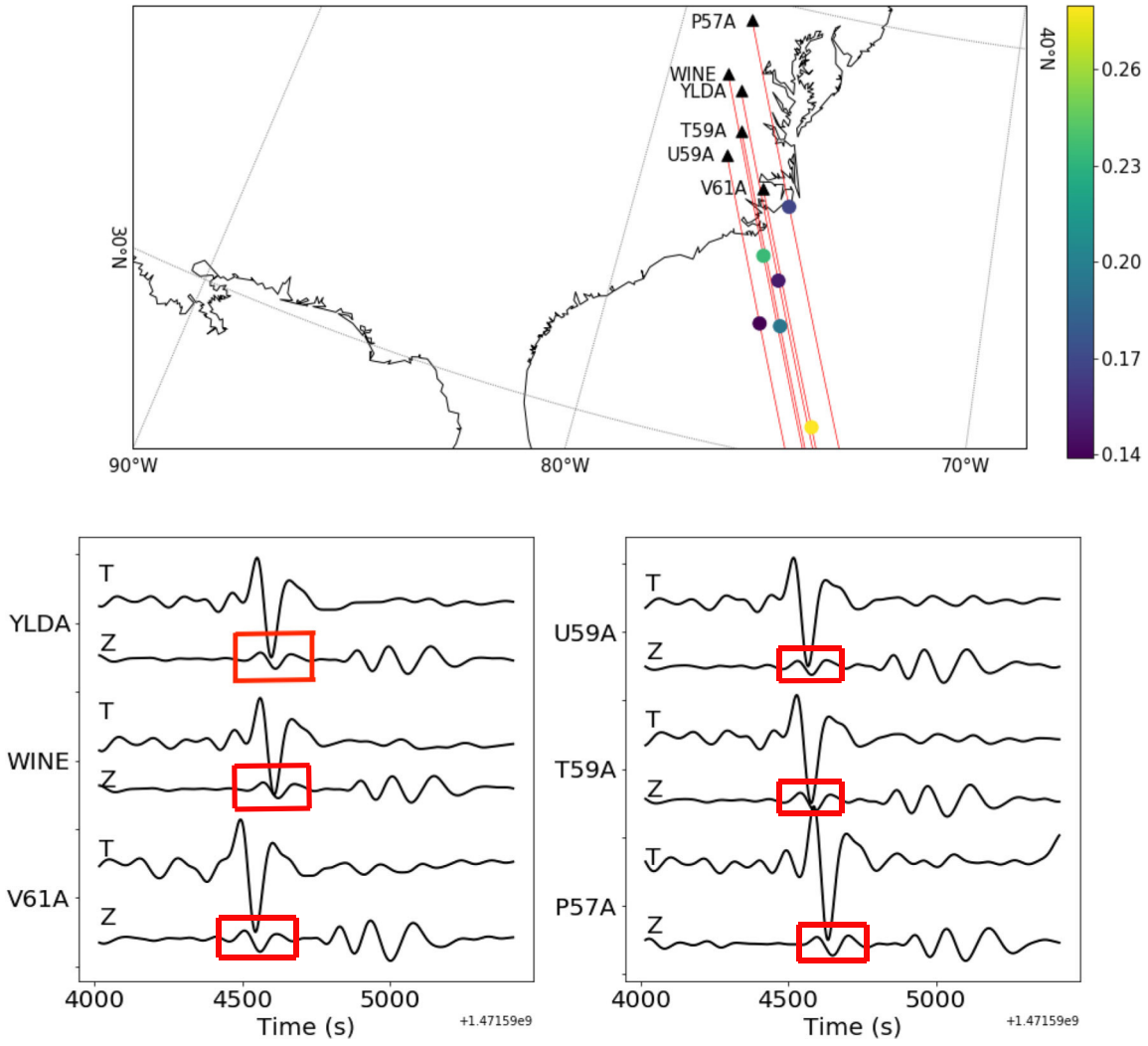

Fig. 4. Example of QL observations for six selected stations (MAGIC stations WINE and YLDA, plus TA stations P57A, T59A, U59A, and V61A) for an earthquake in the Scotia arc. The top panel shows station locations (triangles) and names, along with the great-circle path for each arrival (red line) and the inferred QL scattering point (circles). The color of each circle corresponds to the measured QL amplitude (as a fraction of the main Love-wave amplitude), as indicated by the color bar at right. The bottom panels show data traces at six stations (station names at left) for the transverse component (top trace in each pair, labeled T), showing the Love-wave arrival, and the vertical component (bottom trace in each pair, labeled Z), showing the main Rayleigh-wave arrival as well as the QL phase. QL arrivals on the vertical components are indicated with red boxes. The time axis is labeled with the time since the earthquake. (For interpretation of the references to color in this figure legend, the reader is referred to the web version of this article.)

that the radial component waveforms are typically noisier and more complex than the vertical component waveforms, which is why we rely primarily on the vertical components for QL identification and measurement, following previous work.) We also show, in Fig. 7, a set of (observed and synthetic) waveforms for the same earthquake measured at seven stations that do not show clear QL arrivals (for this particular event) – for these stations, no anomalous arrivals on the vertical component are inferred.

The comparison between data and synthetics shown in Figs. 6 and 7 illustrate that there is significant heterogeneity within our study area as to whether a QL phase is observed or not for a given event. This heterogeneity is likely due to a combination of factors: first, if there are isolated portions of the passive margin that exhibit a sharp lateral transition in anisotropic structure, then for a set of raypaths from a given earthquake, we would only expect the fraction of them that sample the anomaly to exhibit QL phases. Second, the amplitude of the QL phases depends on the azimuth between the wave propagation direction and the axis of anisotropy (Park, 1997), so that maximum scattering is expected for waves that propagate in a direction 45° from the anisotropy axis. Therefore, waves that sample the same region of anisotropy may exhibit different QL amplitudes, or may not exhibit a clear QL arrival at all, depending on the direction of propagation. We note, however, that the amplitudes of the scattered QL waves are expected to vary slowly with azimuth as trigonometric functions (Park, 1997), so minor differences in propagation directions cannot be the sole explanation for large differences in QL amplitudes. Third, our analysis does not explicitly account for three-dimensional wavespeed, anisotropic, or attenuation heterogeneity along the path, or for other complex waveform effects that may distort the waveforms.

Our measurement procedure relies on an assumption of waveform similarity between the Love waves and the scattered QL waves. In order to illustrate the validity of this assumption, we show in Supplementary Figs. S1 and S2 examples of the computation of cross-correlation values between the transverse and vertical components (that is, between the Love and QL arrivals), demonstrating waveform similarity. Fig. S1 shows cross-correlation values for individual waveform examples, while Fig. S2 shows values in map view for a sample event.

Our analysis of 12 earthquakes at ~400 seismic stations in eastern North America yielded a total of 2575 event-station pairs, each of which was visually inspected and processed via the QL measurement

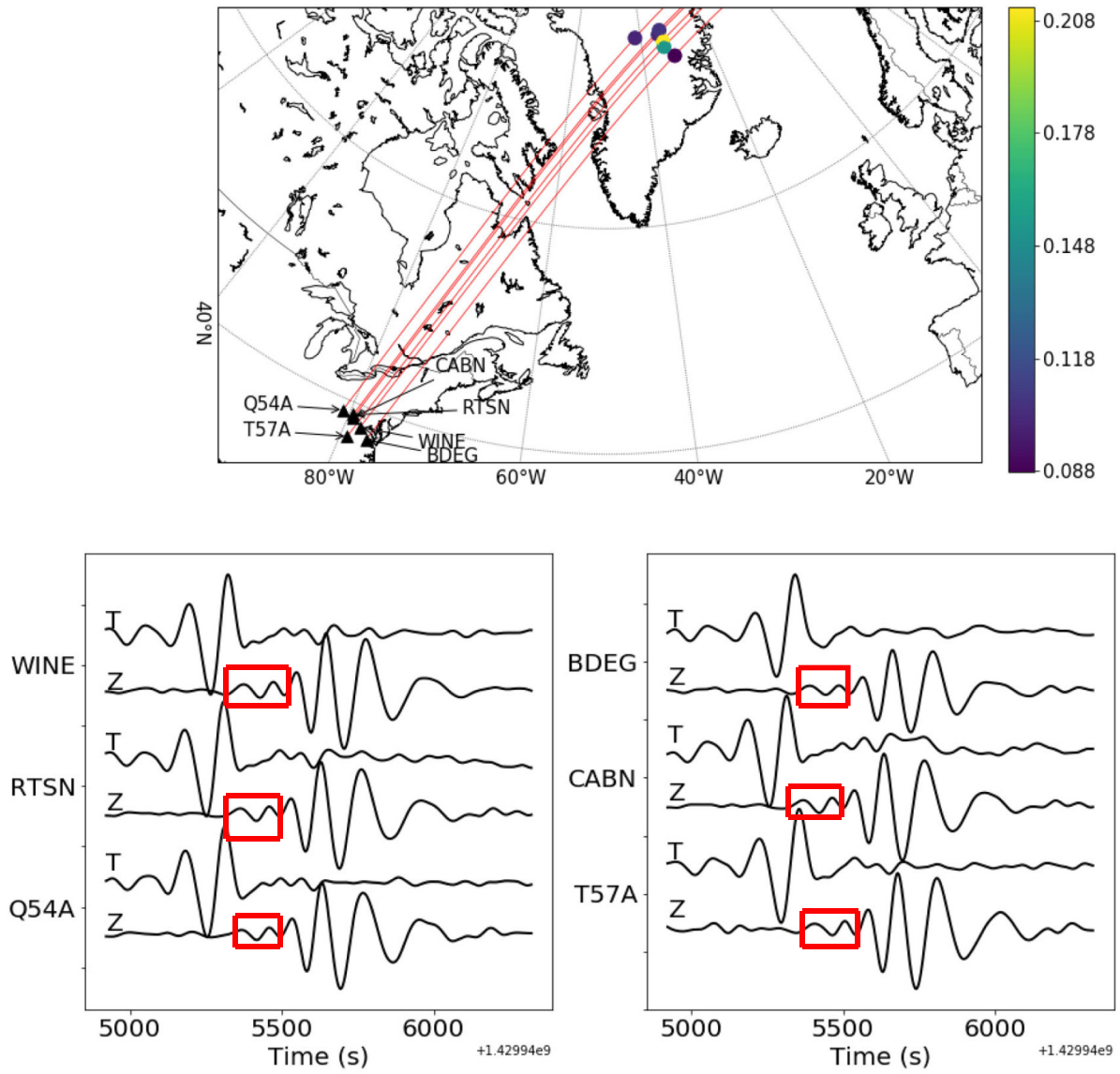

Fig. 5. Example of QL observations for six selected stations (MAGIC stations RTSN, WINE, and WTMN, plus TA stations Q54A, T57A, and X58A) for an earthquake in Nepal. Plotting conventions are as in Fig. 4. Note that several of the scattering points in this figure are nearly co-located.

algorithm described in Section 3.2. Of the 2574 records processed, we identified QL arrivals on 1090 of them, or 42%. The details of each of our QL observations (including station and event information, location of backprojected scattering point, and delay time and amplitude of the QL wave) can be found in Supplementary Table S1. Of the 12 events examined, four show clear, consistent, robust evidence for anisotropic scattering near the east coast of North America (Fig. 8), and four show similarly robust evidence for anisotropic scattering near the southern coast of Greenland (Fig. 9); each of these observations is discussed in detail in Section 3.2 below. Of the remaining four events (Supplementary Fig. S3), two show evidence for sporadic scatterers (one sampling near Greenland, two sampling near ENAM) that are geographically consistent with other observations (Figs. 8 and 9), but for which the scattered phases are weaker and more sporadic. The other two show evidence for anisotropic scattering in the central portion of the Atlantic Ocean. While the latter observation is interesting, and may shed light on the pattern of azimuthal anisotropy beneath the central Atlantic, it is less germane to the focus of this study on the nature of passive continental margins. Therefore, we concentrate our analysis on the seven events that show clear and consistent scattering in either the ENAM region or in southern Greenland. Examples of the cross-correlation values between radial and transverse components are shown in Supplementary Fig. S3, which illustrates cross-correlation coefficients in map view for the September 2013 event (corresponding to Panel B of Fig. 8).

3.2. Two regions of scattering: ENAM and southern Greenland

Fig. 8 shows results from four different earthquakes originating in the southern Atlantic Ocean, each of which shows clear evidence for QL scattering near ENAM. The first of these (Fig. 8A) took place in November 2013 and has waves arriving from an average backazimuth of ~164°, and shows evidence for QL phases measured at a large number (124) of stations in the northern portion of the study area, with few or no observations at stations located in the southern portion. The scattering points consistently map to an east-west trending swath at about 35°N latitude, just offshore the U.S. states of North and South Carolina. Amplitude measurements for the QL phases are mostly between ~10%–20% of the Love-wave amplitude, consistent with previous studies (e.g., Yu et al., 1995; Levin et al., 2007; Rieger and Park, 2010; Margheriti et al., 2014; Chen and Park, 2013). We did measure a small number of anomalously large amplitudes (~50%), which seemed

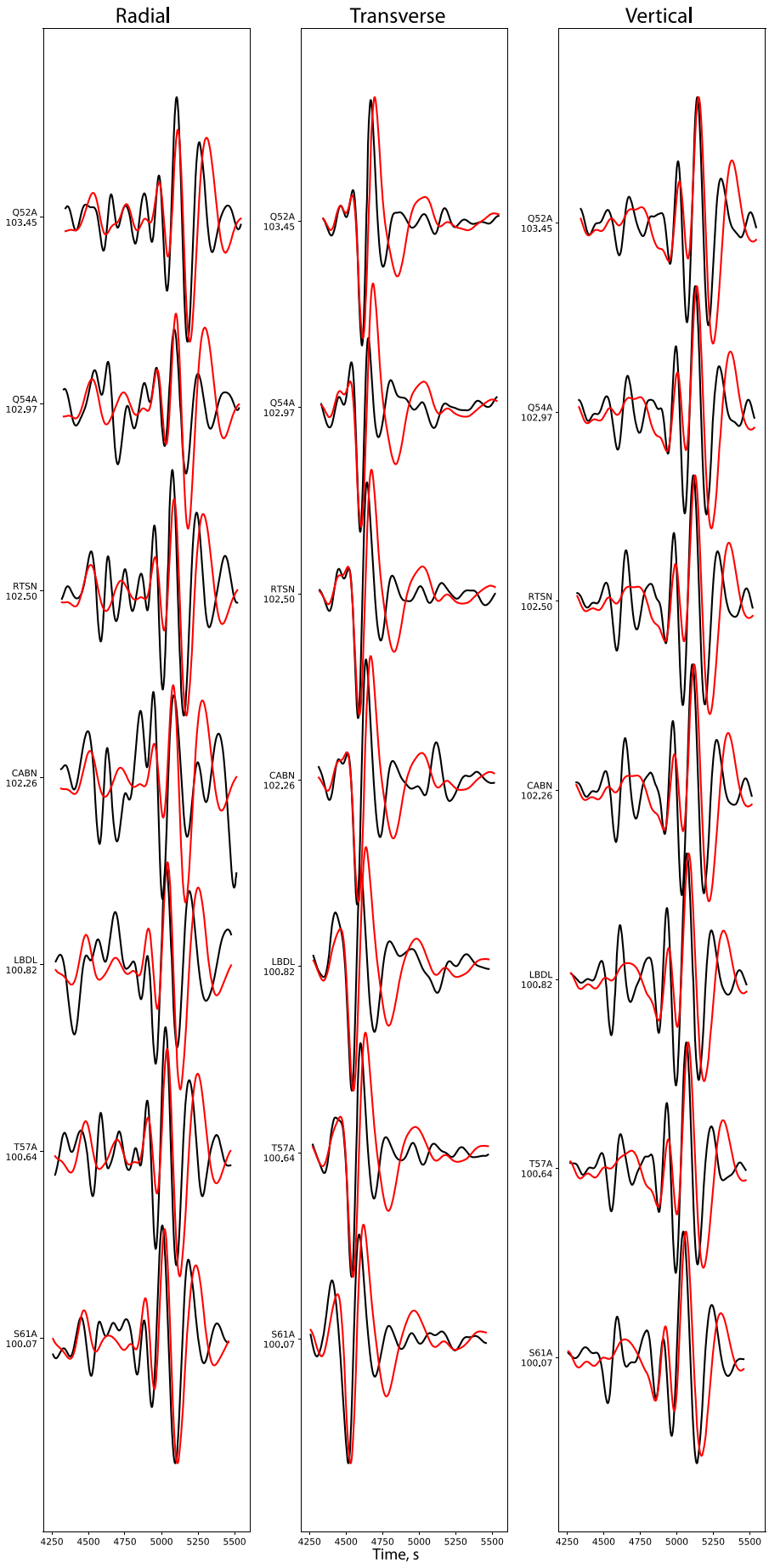

Fig. 6. Comparison between data and synthetic seismograms for a selection of 10 stations in eastern North America that show clear QL arrivals, for an event of magnitude 7.4, on August 19, 2016, located in the Scotia subduction zone. Left panels show radial component seismograms, middle panels show transverse component seismograms, and right panels show vertical component seismograms. Station names are labeled at left, along with epicentral distance values (in degrees). Synthetic traces are shown in red, and data traces are shown in black. For this set of stations, an anomalous QL arrival is clearly visible on the vertical component within the time window associated with the arrival of the Love wave on the transverse component. (For interpretation of the references to color in this figure legend, the reader is referred to the web version of this article.)

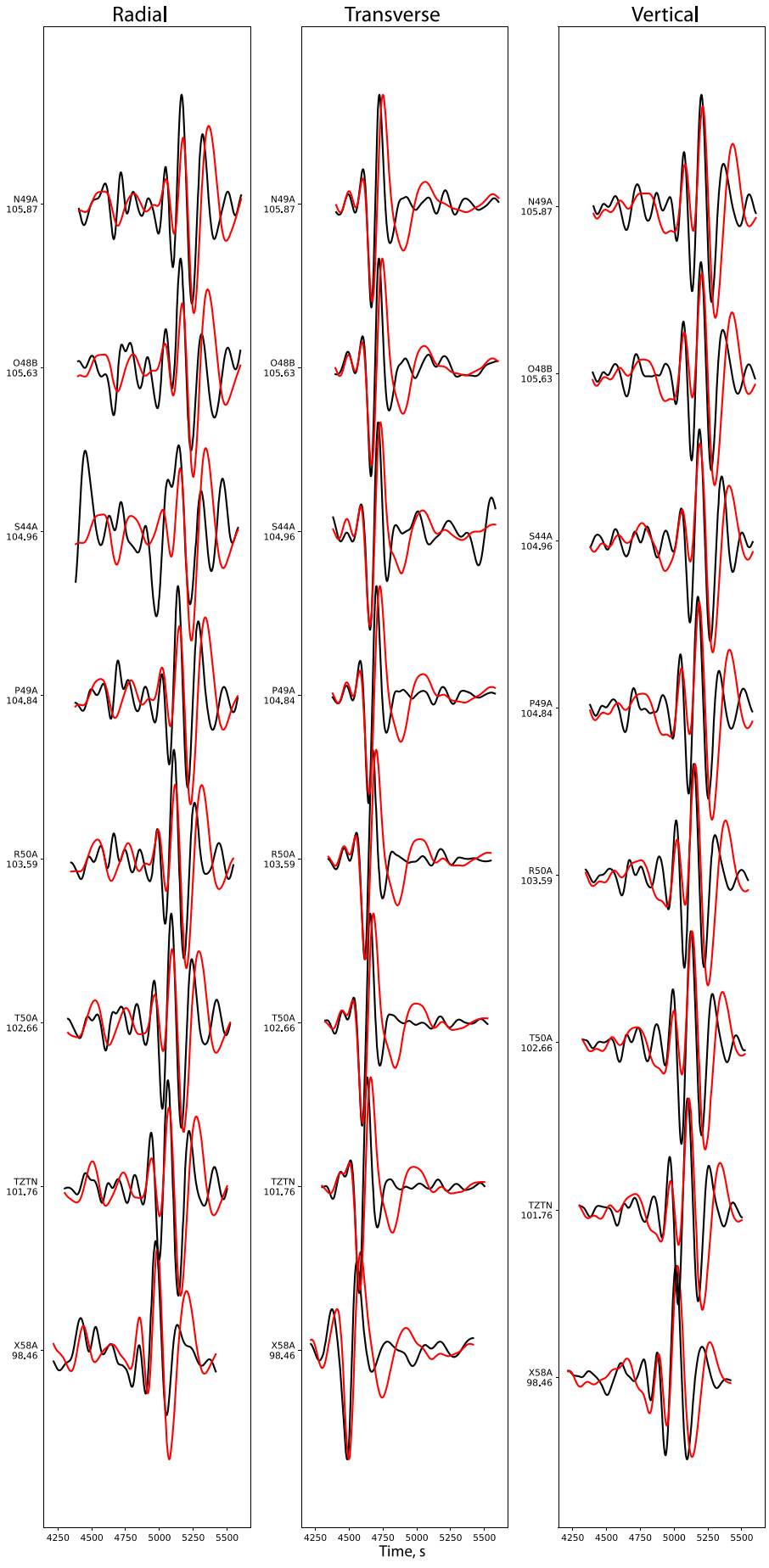

(caption on next page)

Fig. 7. Comparison between data and synthetic seismograms for a selection of 10 stations in eastern North America that do not show clear QL arrivals, for an event of magnitude 7.4, on August 19, 2016, located in the Scotia subduction zone (same event as in Fig. 6). For this set of stations, no clear QL phase is visible on the vertical components. Plotting conventions are as in Fig. 6.

unrealistic. We also measured a modest number of scattering points that lie onshore, although data from this event strongly suggests that the most coherent region of scattering lies just offshore the margin (Fig. 8A).

The next event, shown in Fig. 8B, has waves arriving from a similar backazimuth (155°), although the station coverage is considerably different than the event shown in Fig. 8A. Specifically, this event took place in August 2016; by this time, the USArray TA network had been removed, although N4 network stations remained in place, and stations of the dense MAGIC array were also in place at this time. We observe QL phases at a number (84) of stations in the central and northern part of the study area; in particular, we clearly observe QL phases at stations in the eastern half of the MAGIC array, although stations in the western half do not exhibit clear QL arrivals. The scattering points are for the most part located along ENAM, spanning across the coastline at a similar latitude as for the event in Fig. 8A. As with the previous event, measured QL amplitudes, for the most part, ranged between 5 and 20% of the Love-wave amplitude, with a few sporadic larger measurements that are unlikely to be realistic. While the minor difference in backazimuth for the events shown in Fig. 8A vs. Fig. 8B may play a role in controlling the measured amplitudes, the differences between the two maps are more likely due to differences in station coverage. The regions associated with scattering, and the average amplitudes of the scatterers, are similar between the two figures, although the exact distribution of the scattering points is different. Specifically, a larger proportion of the mapped scattering points lie onshore in Fig. 8B.

The third ENAM-sampling event, shown in Fig. 8C, occurred in late 2016, after the MAGIC stations had been removed. This event was therefore measured by a smaller number of stations, mostly from the N4 network. For this event, QL phases were observed for a group of stations in New England, with sporadic observations of scattered waves for stations to the south and west, and a few observations for stations in the westernmost part of the study area. For the first group of stations, the scatterers map to a region offshore the central portion of ENAM, near the eastern end of the group of scatterers shown in Fig. 8A. Another coherent group of scatterers emerges in the Gulf of Mexico, from QL phases measured at stations in central North America. We note that this event was located closer to the stations (that is, at a shorter range of epicentral distances) than other events in our data set; therefore, there was a shorter time separation between the main Love and Rayleigh arrivals, and QL arrivals were more difficult to identify based on visual comparison between synthetic and observed waveforms. As with other

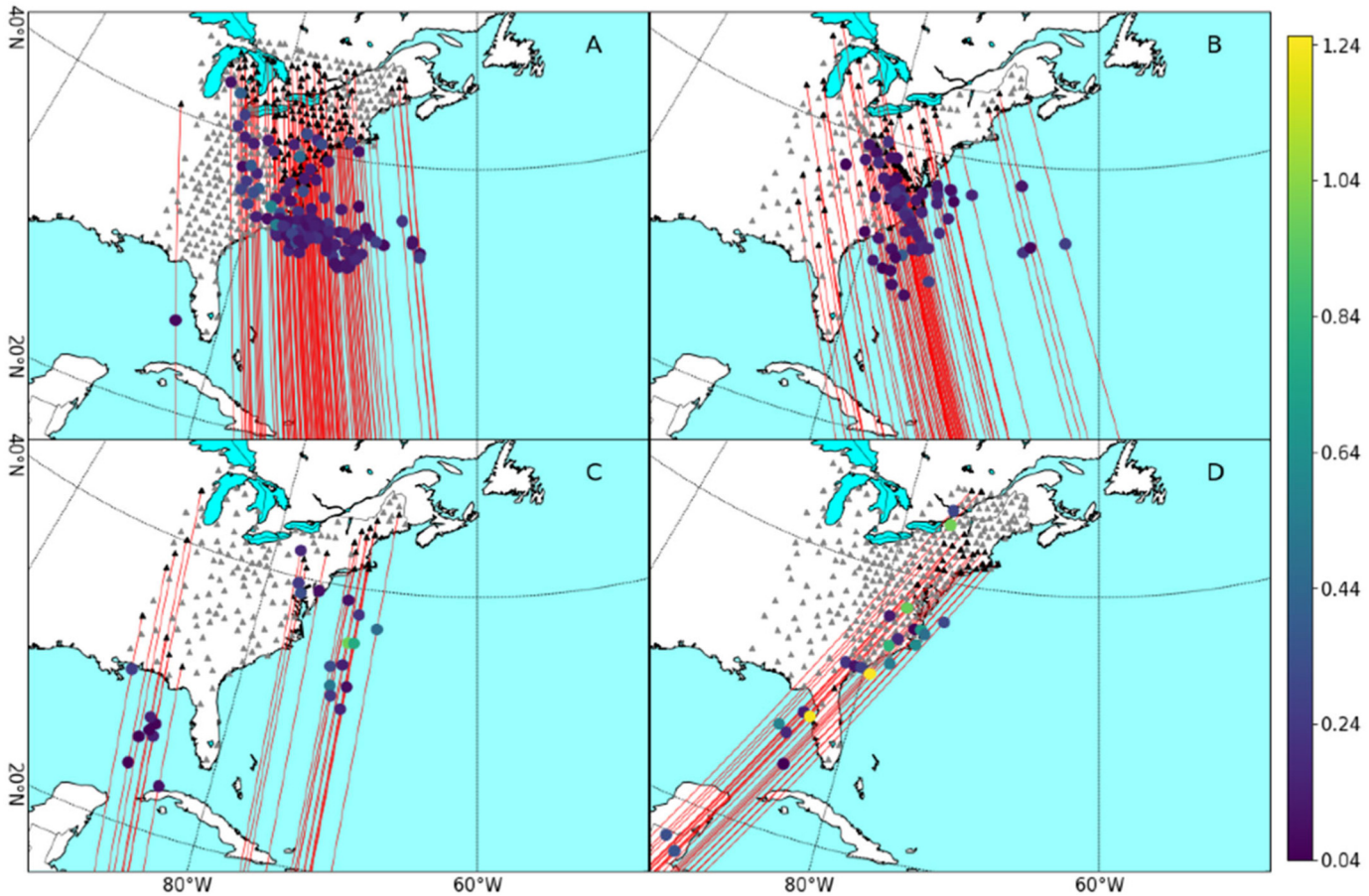

Fig. 8. Scattering maps for individual events that show QL generation along ENAM. Each panel shows the stations that were operational at the time of the event (triangles). Stations that showed a QL arrival are shown in black, while stations that showed no QL arrival are shown in gray. Great-circle paths for those arrivals that showed a clear QL phase are shown with red lines, and the associated scattering points are shown as circles. The color of each circle corresponds to the amplitude of the QL phase, as shown in the color bar at left. Panel A shows an event in November 2013, panel B shows an event in August 2016, panel C shows an event in December 2016, and panel D shows an event in October 2014 (see event information in Table 1). (For interpretation of the references to color in this figure legend, the reader is referred to the web version of this article.)

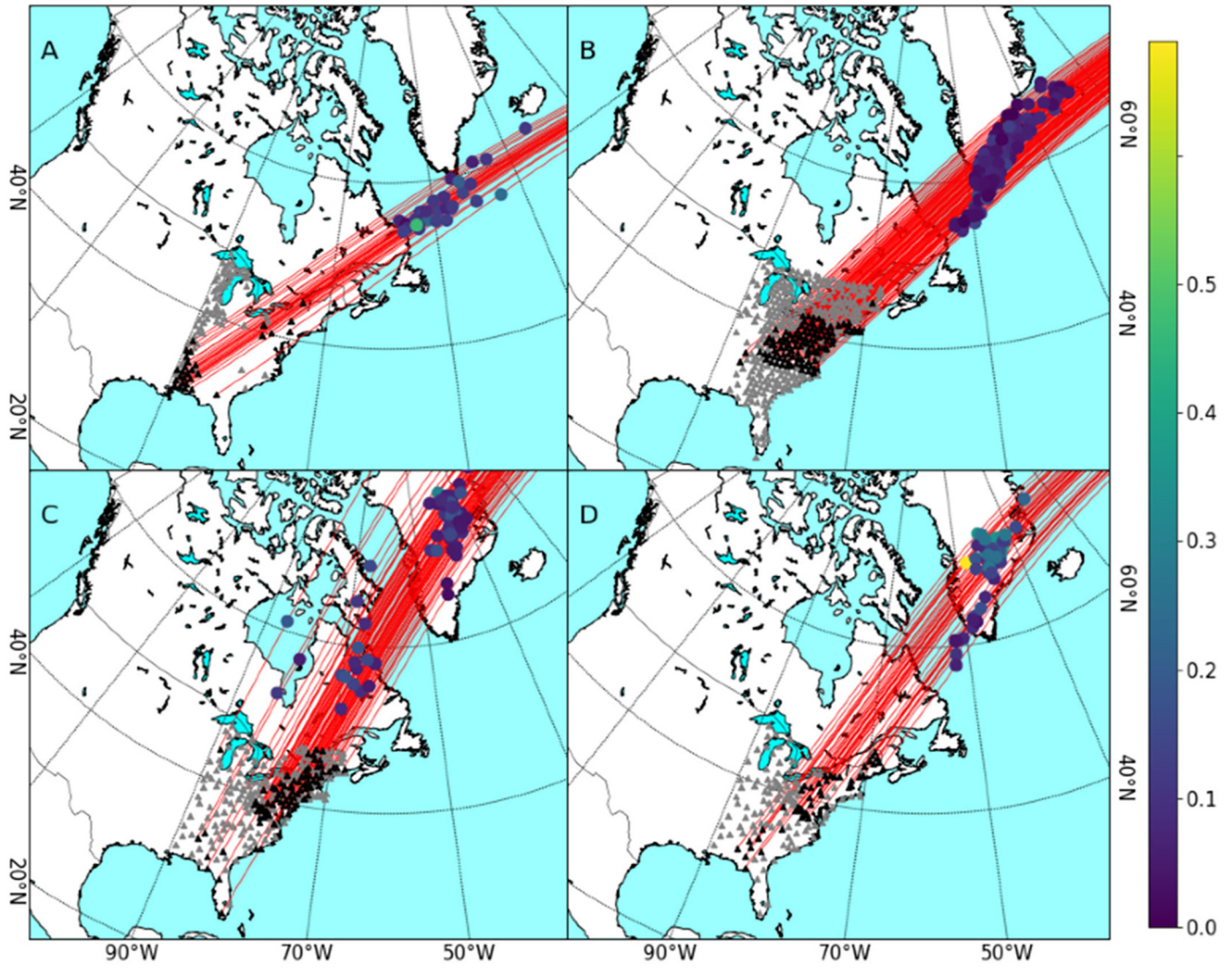

Fig. 9. Scattering maps for individual events that show QL generation near central or southern Greenland. Plotting conventions are as in Fig. 8. Panel A shows an event in October 2011, panel B shows an event in September 2013, panel C shows an event in April 2015, and panel D shows an event in December 2015 (see event information in Table 1).

events, there are a few unrealistically large estimated amplitudes in Fig. 8C.

A fourth event, shown in Fig. 8D, originated at the southern East Pacific Rise, and thus arrives at eastern North American stations at a different azimuth than the other events shown in Fig. 8 (arriving from the southwest). Many of the stations examined did not show QL scattering for this raypath geometry. We did, however, observe QL phases at a group of stations located mostly in and around New England, with the scattering points generally mapping near the coast of the Carolinas, with a few located to the west and south of Florida. We note that this event had a magnitude (7.2) on the smaller end of the range of magnitudes examined in this study, and the signal to noise ratios were therefore smaller for this set of waveforms than for other events in the dataset. Again as with other events, there are a few unrealistically large estimated amplitudes in Fig. 8D. Taken together, the four events that sample ENAM well all suggest a coherent region of anisotropic scattering in the central portion of ENAM, which crosses the U.S. shoreline at the latitude of the Carolinas and extending offshore. Interestingly, this region corresponds to the study area of the GeoPRISMS ENAM CSE, as discussed further below.

Although it was not an initial focus of our study, our measurements have also revealed an unexpected locus of QL scattering in the vicinity of southern Greenland. This region was sampled by waves originating from earthquakes in and around the Himalayas. Analysis of data from four different events yielded clear and convincing evidence for QL phases scattered from an anisotropy gradient near southern Greenland (Fig. 9). The first of these (Fig. 9A) was an earthquake in October 2011 that occurred before many of the stations used in our study had been deployed, but was clearly recorded at USArray stations in the western portion of our study area. Of these stations, those located in the southern portion of the U.S. showed clear QL arrivals, while those in the central and northern portions did not. Given the relatively large delay time between the Love and QL arrivals, the corresponding scattering points are located just offshore the southern tip of Greenland (Fig. 9A). Measured QL amplitudes, for the most part, ranged between ~5%–25%. As with other events, there were a few sporadic measurements of unrealistically high amplitudes. The next event (Fig. 9B) occurred in September 2013 and exhibited clear QL arrivals (amplitudes between ~5%–18%) throughout much of the study region, again with scattering points located offshore the southeastern coast of Greenland.

The third event (Fig. 10C) is the April 2015 Gorkha earthquake in Nepal, notable for its large magnitude (Mw = 7.9), complex source processes, and considerable damage near the earthquake epicenter (e.g., Grandin et al., 2015; Denolle et al., 2015; Fan and Shearer, 2015).

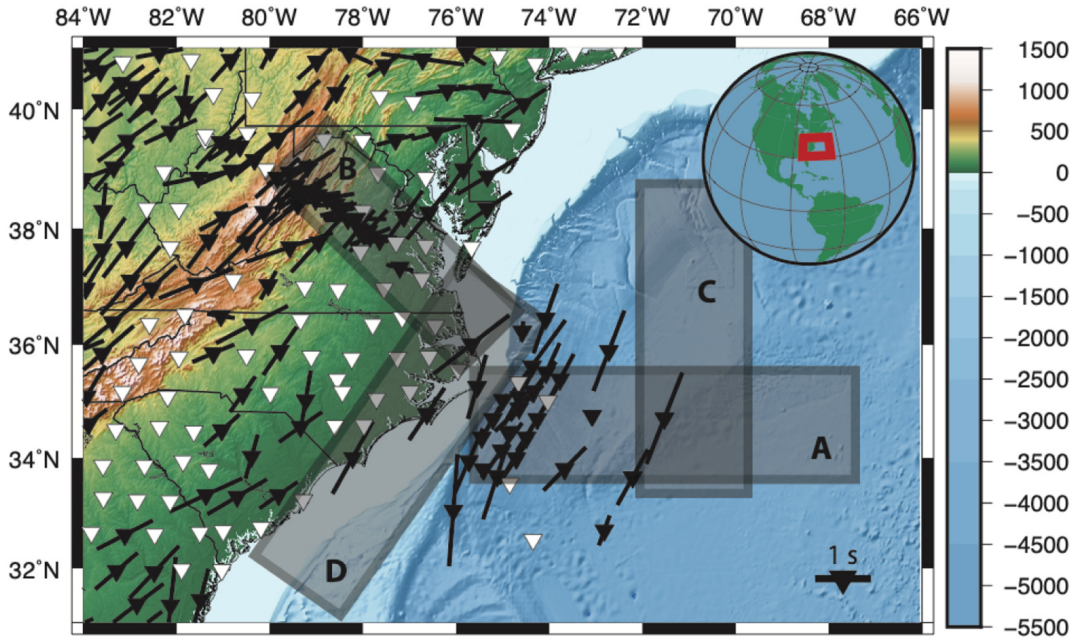

Fig. 10. Comparison between SKS splitting results beneath the ENAM margin (from previous work) and QL scattering results (from this study). Inset shows location of main map on the globe. We show single-station (station locations shown with triangles) average SKS splitting parameters from the work of Long et al. (2016) for TA stations, from Aragon et al. (2017) for stations of the MAGIC array, and from Lynner and Bodmer (2017) for the offshore stations of the ENAM CSE. Splitting parameters are indicated with black bars, with the orientation of the bar corresponding to the fast splitting direction and the length of the bar corresponding to the delay time (as shown by the scale bar at bottom right). Stations shown with white triangles were either dominated by null measurements, or did not yield high-quality results. Regions that generate consistent QL scattering for the events shown in Fig. 8 are indicated with gray shading and are labeled A-D. Box A corresponds to scattering points generated by the event shown in Fig. 8A. Box B corresponds to scattering points generated by the event shown in Fig. 8B. Box C corresponds to scattering points generated by the event shown in Fig. 8C. Box D corresponds to scattering points generated by the event shown in Fig. 8D; the event in Fig. 8A also caused significant scattering in this geographic region.

Waves from this event arrived at eastern North America stations from a backazimuth of ~14° and passed through the southern half of the Greenland landmass. Again, QL phases were observed at a relatively large number of eastern North American stations (87), most in the central and northern portion of the study area, including most stations of the MAGIC array (Fig. 9C). The scatterers for this event were generally located in the central and southern portion of Greenland, further north than the group of scatterers observed for our earlier events (Fig. 9A and B). We also observed some scattering points located beneath northeastern Canada. Finally, arrivals from a fourth event (Fig. 9D) in December 2015, coming from a similar backazimuth as those from the Gorkha earthquake (~21°), show a very similar pattern of scattering, with stations in the central and northern portions of our study area (and a few in the south) exhibiting QL phases. As with the Gorkha event, the scattering points lie in the southern portion of the Greenland landmass. Taken together, observations from the four earthquakes shown in Fig. 9 provide robust evidence for lateral gradients in azimuthal anisotropy beneath the southern part of Greenland and the region just offshore Greenland's southeastern coast.

4. Discussion

4.1. Errors and uncertainties on delay times, amplitudes, scattering points, and interpretation

A key consideration for this work is the nature and size of the uncertainties in the calculated scattering points. Chen and Park (2013) carried out a numerical experiment to generate synthetic seismograms for a simple anisotropic model and showed that the cross-correlation method of measuring QL delay times was sufficiently accurate to retrieve the locations of scattering points to within approximately 50–100 km for data with dominant periods of 100 s. This numerical experiment, however, was carried out using a simplified anisotropic Earth model and noise-free synthetic waveforms. In the real Earth, there are several factors ignored by our analysis that contribute to relatively large uncertainties when estimating scattering point locations and QL amplitudes. These include our use of ray theory in calculating the wave paths and our neglect of possible contributions from off-path structure, multiple scatterers, the effects of anelasticity on wave propagation, and wavespeed heterogeneity in calculating the great-circle paths. While the numerical experiment of Chen and Park (2013) suggests that the uncertainties associated with the actual delay time measurements (via cross-correlation) are themselves relatively modest, other factors likely contribute to the overall uncertainty in scattering point location. We estimate that the scattering points are likely well constrained to within a few hundred km, but we hesitate to interpret our scattering point maps on length scales smaller than that.

In our interpretation, we considered whether surface wave multipathing, or other scattering effects due to isotropic boundaries, might contribute to our observations. Previous studies have demonstrated multipathing for Rayleigh waves along the west coast of North America, with later wave packets arriving after the main Rayleigh wave (Ji et al., 2005). Surface wave scattering due to isotropic structure was also documented by Yu et al. (2017), who showed that SH waves scatter to Love waves due to the (isotropic) structure beneath the Southern California continental borderland. While they cannot be ruled out, isotropic scattering and multipathing effects are unlikely to be the primary explanation for the QL waves documented in this study, as the scattering of Love to Rayleigh energy requires gradients in seismic anisotropy (Park, 1997). The fact that we observe Rayleigh waves in the time window between the arrival of the Love waves and the main Rayleigh waves (but long after the arrival of relevant body wave phases) implies that a gradient in anisotropy beneath our study region is needed to explain our observations.

4.2. Depth distribution of the inferred anisotropy

The surface waves examined in this study have a dominant period of ~100 s. Calculations of the depth sensitivity of cross-mode coupling between toroidal and spheroidal modes with periods near 100 s indicate that the maximum sensitivity is near a depth of ~150 km, with significant sensitivity over the ~100–200 km depth range and at least some sensitivity to upper mantle structure outside of this depth range (Chen and Park, 2013; see their Fig. 9). Beneath our study region on the edge of a passive continental margin, the depth of maximum sensitivity (~150 km) corresponds to asthenospheric upper mantle beneath the oceans (where the maximum depth of the lithosphere is ~100 km; e.g., Fischer et al., 2010). Beneath the continent, however, it is more ambiguous as to whether QL observations are more sensitive to anisotropy in the lithospheric mantle, in the asthenosphere, or a combination of the two. In continental interiors, the lithosphere can be as much as ~200–250 km thick (e.g., Fischer et al., 2010), so QL scattering within continental interiors likely reflects lithospheric anisotropy and deformation (e.g., Chen and Park, 2013). Along passive continental margins, however, the lithosphere is often thinner, perhaps reflecting thinning during extension associated with continental rifting during supercontinent breakup. Observations of the lithosphere-asthenosphere boundary (LAB) by Rychert et al. (2007) beneath the northeastern U.S. reveal a lithospheric thickness of ~100 km. Closer to our study region, Evans et al. (2019) found evidence for thin lithosphere (~70–80 km) beneath the central Appalachian Mountains, with somewhat thicker lithosphere (~120 km or perhaps greater) beneath the Coastal Plain to the east. In the southeastern portion of the U.S., magnetotelluric data has been interpreted as requiring a thick (~200 km or more) lithospheric root beneath the Coastal Plain (Murphy and Egbert, 2017). While reconciling this result with seismic velocity models based on surface wave tomography is not entirely straightforward, it is possible when anelastic effects are considered (Murphy and Egbert, 2019).

In any case, for scattering points that map to the onshore portion of the passive margin, it is ambiguous as to whether the observations reflect anisotropy in the asthenospheric upper mantle, the lithosphere, or (most likely) a combination of the two. For scattering points that map at or near the coastline, it is plausible that the generation of QL phases is related to the contrast between anisotropy in the asthenospheric upper mantle beneath the oceanic plate just offshore, and anisotropy either in the mantle lithosphere or in the sublithospheric mantle onshore (depending on the local lithospheric thickness value). For scattering points that map well offshore, QL phases may mainly reflect a lateral contrast in anisotropy within the asthenospheric upper mantle. In all cases, it is important to keep in mind that sensitivity kernels for cross-mode coupling at 100 s (Chen and Park, 2013) indicate that sensitivity is distributed throughout the upper mantle, with significant sensitivity throughout the 100–200 km depth range, and so possible contributions from both the lithosphere and the asthenosphere should be taken into account.

4.3. Comparison with previous anisotropy studies

Because QL observations provide constraints on upper mantle anisotropy that are complementary to those provided by SKS splitting measurements, it is instructive to compare our results to SKS splitting observations and to surface wave tomography models that include azimuthal anisotropy. We first consider southern Greenland, which displays robust Love-to-Rayleigh scattering (Fig. 9). Observations of splitting beneath Greenland are relatively sparse, and mostly limited to coastal regions, but a few studies have explored upper mantle anisotropy using SKS measurements (Ucisik et al., 2005, 2008). In particular, Ucisik et al. (2008) documented a sharp transition in SKS fast splitting directions between the northern portion of Greenland and its southern portion. It is possible that this transition is contributing to the scattering observations shown in Fig. 9C and D, although our raypaths are effectively propagating nearly parallel to this boundary, rather than across it. Inferences on lithospheric thickness beneath central and southern Greenland are not particularly consistent, with receiver function studies suggesting that it is thin (~80 km; Kumar et al., 2009) and surface-wave studies suggesting a thick (and anisotropic) lithospheric keel of at least ~120 km (Darbyshire et al., 2018). It is ambiguous, therefore, whether the transitions in anisotropy suggested by our QL observations beneath Greenland lie within the lithospheric mantle, the asthenosphere, or both. Darbyshire et al. (2018) suggested that the lithospheric mantle beneath Greenland has been heterogeneously deformed by past tectonic episodes during the assembly and evolution of the continent, an argument that provides a possible mechanism for lateral transitions in anisotropy that might give rise to QL phases. Another intriguing possibility is that the asthenospheric upper mantle beneath Greenland has accumulated a relatively strong, anisotropic texture via successive cycles of postglacial isostatic rebound, which has been considerable in this region (e.g., Huybrechts, 2002). It is unclear, however, whether hysteresis associated with glacial-uplift cycles would be large enough to produce significant texture, or whether successive deformation episodes would cause texture to reset. In any case, our measurements suggest that there is substantial heterogeneity in upper mantle anisotropy beneath the central and southern part of Greenland, and this represents an interesting target for future study.

While not the main focus of this paper, we also note the intriguing observation of QL phases that are apparently generated by anisotropic gradients in the central Atlantic Ocean (Supplementary Fig. S3). The detailed pattern of azimuthal anisotropy beneath the Atlantic Ocean basin is not well understood, because of the dearth of seismic stations located within the oceanic region. Global azimuthal anisotropy models derived from surface wave measurements (e.g., Debayle and Ricard, 2013) hint at some complexity in the anisotropy patterns in the central Atlantic basin, but the resolution of these global models is relatively coarse. A (presumably) localized disturbance of the basin-wide upper mantle flow field beneath Bermuda, in the form of vertical upwelling in the asthenospheric upper mantle, was suggested by Benoit et al. (2013). This suggestion was based on a documented lack of SKS splitting (consistent with vertical mantle flow) measured at a seismic station on Bermuda; subsequent geochemical work (Mazza et al., 2019) has also provided support for the idea of localized upwelling beneath the region. We speculate that the Love-to-Rayleigh scattering generated beneath the Atlantic Ocean Basin documented in Fig. S3 is related to this localized mantle upwelling, and/or to the complexity in azimuthal anisotropy structure suggested by the models of Debayle and Ricard (2013). Again, while our QL observations cannot tightly constrain the geometry of, or mechanism for, the gradient in anisotropy, they do suggest that the Atlantic Ocean basin would be an interesting target for future work.

In contrast to Greenland and the central Atlantic Ocean basin, there are a plethora of recent studies of upper mantle azimuthal anisotropy beneath ENAM, including those based on SKS splitting measurements (Long et al., 2016; Aragon et al., 2017; Yang et al., 2017; Lynner and Bodmer, 2017) and those based on surface wave measurements (Wagner et al., 2018). Long et al. (2016) and Yang et al. (2017) both examined SKS splitting at TA stations, and found evidence for complex and laterally variable patterns of both fast directions and delay times. Long et al. (2016) interpreted these patterns as reflecting a combination of lithospheric and asthenospheric anisotropy, with orogen-parallel fast directions throughout the Southern and Central Appalachian Mountains, and predominantly null SKS arrivals observed at stations located on the Coastal Plain of the southeastern U.S. Yang et al. (2017) documented patterns that were generally similar to those found by Long et al. (2016) throughout eastern North America, although one exception was their finding of generally NNE-SSW fast directions, with relatively low delay times, in the region of null splitting identified by Long et al. (2016). These differences are likely due to differences in the frequency content, preprocessing procedures, and measurement

strategies between the two studies. Aragon et al. (2017) measured SKS splitting at stations of the dense MAGIC experiment and documented generally NE-SW fast directions through most of the array, with a sharp transition to more E-W fast directions to the east of the Appalachian Mountains (beneath the Coastal Plain). Lynner and Bodmer (2017) measured SKS splitting for broadband stations of the ENAM CSE, and found striking, consistent, margin-parallel fast splitting directions, contrasting both with the weaker and more complex splitting beneath the Atlantic Coastal Plain onshore just to the west, and with the simplest expectation that fast splitting directions would tend be parallel to absolute plate motion beneath oceanic plates. Finally, Wagner et al. (2018) generated azimuthally anisotropic phase velocity maps beneath the southeastern U.S. from surface wave dispersion observations; strikingly, they found evidence for generally weak and complex anisotropy, with fast directions that varied both laterally and with depth. At long periods (100–125 s), the phase velocity maps of Wagner et al. (2018) show very weak anisotropy beneath the Atlantic Coastal Plain region.

How do our inferences of lateral gradients in anisotropy compare to the constraints on anisotropy provided by these earlier studies? Fig. 10 shows a map of SKS splitting observations for the southeastern U.S. from Long et al. (2016) and Aragon et al. (2017) for the onshore portion, and Lynner and Bodmer (2017) for the offshore portion, along with a schematic diagram of QL scattering point locations from this study. Taken together, these observations reveal a region of substantially complex anisotropy in the upper mantle. The splitting observations suggest a number of lateral transitions in upper mantle anisotropy, including (from west to east) changes from clearly orogen-parallel fast directions beneath the Appalachian Mountains, to weak and complex anisotropy beneath the Coastal Plain (perhaps with a component of vertical flow in the asthenosphere, as suggested by Long et al., 2010), to clear margin-parallel fast directions beneath the ENAM CSE study region. While we lack well-resolved constraints on upper mantle anisotropy beneath the Atlantic Ocean basin to the east of the ENAM CSE, the global model of Debayle and Ricard (2013) hints at some complexity in azimuthal anisotropy beneath this region. This may suggest a further transition from margin-parallel fast directions near the coast, as delineated by Lynner and Bodmer (2017), to a different regime of azimuthal anisotropy further to the east.

When we compare the location of our mapped scattering points to the SKS splitting patterns (Fig. 10), it is clear that QL observations made in this study potentially sample a number of these transitions. For two of the events shown in - Fig. 8 (2013-11-17 and 2016-12-25; Fig. 8A and C), most of the scattering points lie offshore, near the region of the ENAM CSE (and to its west). Beneath this region, the oceanic lithosphere is likely relatively thin (less than 100 km), and thus the depth of peak sensitivity of Love-Rayleigh coupling at 100 s lies in the asthenospheric upper mantle. This argues for at least some component of complex flow in the asthenosphere, with a relatively sharp lateral gradient along the ray path. The ray propagation direction for waves that originate from earthquakes in and around the Scotia Arc and are measured in eastern North America lies at an oblique angle (roughly ~50–60°) to the fast directions documented by Lynner and Bodmer (2017), so it is plausible that the anisotropy in the upper mantle beneath the ENAM CSE region is contributing to the generation of QL phases in our data set. For a third event in Fig. 8 (2016-08-19), the set of scattering points seem to cross the shoreline, with some located offshore and some located onshore, beneath the Coastal Plain or the Appalachian Mountains. In this case, the QL phases may reflect the transition between the relatively strong margin-parallel fast anisotropy offshore (Lynner and Bodmer, 2017) and the relatively weak anisotropy beneath the Coastal Plain (Long et al., 2016; Aragon et al., 2017). A few scattering points (Fig. 8B) are mapped further inland, in and around the Appalachian Mountains. For this subset of observations, it is plausible that the transition from weak anisotropy beneath the Coastal Plain to more coherent anisotropy at lithospheric depths beneath the Appalachians may be contributing to the observed scattering.

4.4. Implications for the structure and dynamics of the ENAM passive margin

Previous work on SKS splitting and anisotropic surface wave phase velocity maps has suggested complex anisotropic structure at the edge of the ENAM passive margin, particularly at latitudes between roughly ~32–40°N (corresponding to the states of Virginia, North Carolina, and South Carolina). This finding is borne out by our observation of QL phases at TA stations within ENAM. It is notable that for events originating in and around the Scotia subduction zone, whose ray paths collectively sample the entire margin (Fig. 8), the vast majority of the identified scattering points lie in and around the central portion of the margin. While there are some exceptions (e.g., the sporadically observed scattering points to the north of the main group in Fig. 8A), it is clear that the scattering points are concentrated in this particular region of ENAM. This suggests that there may be something unique about the anisotropic structure of the lithospheric mantle, the asthenosphere, or both beneath this portion of the margin. This, in turn, suggests either a unique history of lithospheric deformation, a perturbation in the present-day flow field in the asthenospheric upper mantle, or a combination of the two.

There are several possible scenarios that may explain why this portion of the margin exhibits particularly complex anisotropic structure that finds expression in the generation of QL waves. One possibility is that this region is undergoing small-scale or edge-driven convection, yielding a relatively localized perturbation to the larger-scale asthenospheric flow field. The concept of edge-driven convection, in which gravitational instability at the edge of thick, cold, dense continental lithosphere drives downwelling and associated upwelling return flow, was proposed by King and Anderson (1998) and has been further explored by King and Ritsema (2000), King (2007), and Kaislaniemi and van Hunen (2014), among others. The possibility of edge-driven convection beneath the southeastern U.S. has been previously explored by King (2007) and Long et al. (2010); the latter noted that the dominantly null SKS splitting observed beneath the Coastal Plain region in Virginia and the Carolinas (Fig. 10) could reflect predominantly vertical mantle flow, perhaps corresponding to the downwelling limb of a small-scale convection cell. King (2007) speculated that the Bermuda hotspot and swell might correspond to the hypothetical upwelling limb of this convection cell; Benoit et al. (2013) found some observational support for this idea by documenting dominantly null SKS splitting beneath Bermuda (again consistent with vertical mantle flow).

A related hypothesis is that lithospheric removal beneath the central Appalachian Mountains has resulted in a localized perturbation to the large-scale mantle flow field. A unique aspect of this portion of the Appalachians is the appearance of anomalously young (~50 Ma) volcanic rocks in western Virginia and eastern West Virginia (Mazza et al., 2014, 2017). Mazza et al. (2014) proposed a lithospheric removal model to explain the presence of these volcanics, with asthenospheric upwelling and decompression melting following the loss of lithosphere due to gravitational instability. Recent observational support for thinned lithosphere beneath the Central Appalachians has come from seismic tomography (e.g., Schmandt and Lin, 2014; Wagner et al., 2018), seismic attenuation measurements (Byrnes et al., 2019), and a combination of receiver-function analysis and an electrical conductivity model (Evans et al., 2019). It is likely that the anomalously thin lithosphere beneath the central Appalachians plays a role in perturbing the asthenospheric flow field, as the North American Plate moves over the mantle beneath (e.g., Evans et al., 2019). A similar set of processes was explored in the context of the Atlas Mountains of Morocco (also located along a passive margin) by Kaislaniemi and van Hunen (2014), who delineated two different styles of edge-driven convection whose interplay produces lithospheric thinning and melting. One question, however, is whether the small-scale convection that may be produced

by (or that may have resulted in) the thinned lithosphere beneath western Virginia is spatially extensive enough to explain the QL scattering over the fairly large area observed in this study.

Another related hypothesis for asthenospheric mantle flow in the region in which we observe QL scattering was proposed by Lynner and Bodmer (2017), who invoked three-dimensional mantle flow beneath the region, with a component of flow parallel to the margin just offshore and a region of vertical flow beneath the Coastal Plain onshore. They further pointed out that the relatively limited offshore data (limited to the footprint of the ENAM CSE; Fig. 10) cannot completely constrain the 3D flow field. Our observations of QL scattering in and around the region of the ENAM CSE study area thus provides an independent line of evidence in support of some type of three-dimensional flow regime in the asthenospheric mantle beneath this portion of the margin. Future work that explores whether QL phases are observed at the offshore stations of the ENAM CSE should help to shed additional light on this possibility.

Finally, another potential scenario that could explain our QL scattering results invokes the presence of lateral gradients in frozen-in lithospheric anisotropy. It is plausible that there are several distinct regimes of lithospheric anisotropy beneath the region of QL scattering identified in this study. These include the oceanic lithosphere offshore the margin, the lithosphere beneath the Coastal Plain, which may be anomalously thick and have unusual physical properties (Murphy and Egbert, 2017, 2019), and the lithosphere beneath the Appalachian Mountains and the central part of the North American continent. Based on changes in shear wave splitting behavior over relatively short length scales beneath the MAGIC array, Aragon et al. (2017) suggested that there is a lateral transition in lithospheric anisotropy from the Appalachian Mountains to the Coastal Plain beneath Virginia. Preliminary observations from the active source component of the ENAM CSE suggest that the oceanic lithosphere beneath the study region may exhibit margin-parallel fast directions, similar to the observed SKS splitting (Shuck and van Avendonk, 2016). While it is plausible that these likely transitions in lithospheric anisotropy contribute to the QL scattering documented in this study, it is unlikely that all of the observed signal can be attributed to the lithosphere, particularly for the scattering points that lie offshore. Given that much of the sensitivity of QL scattering is to structure in the depth range between ~100–200 km, it is unclear whether the ~100 km thick oceanic lithosphere can be the main source of the signal. Nevertheless, it is certainly possible that lateral transitions in anisotropy within the lithosphere may contribute to the QL observations we document.

5. Summary

We have processed a large amount of broadband seismic data from stations located in eastern North America and found evidence for Love-to-Rayleigh scattering, in the form of quasi-Love (QL) waves. This scattering implies strong lateral gradients in azimuthal anisotropy in the upper mantle. Our analysis reveals two significant geographic loci of Love-to-Rayleigh scattering, with one region in and around southern Greenland, and one region just offshore ENAM, with strong scattering both offshore and just onshore at latitudes of 32–40°N. The latter region coincides with the GeoPRISMS ENAM CSE study area, and therefore SKS splitting measurements are available for this offshore region. These previous measurements had suggested a transition from margin-parallel flow in the asthenospheric upper mantle just offshore ENAM to more vertical flow beneath the onshore portion of the margin. Our mapped scattering points are consistent with the scenario in which QL waves are generated either at this transition, or at the transition between localized margin-parallel flow and flow that may be controlled by absolute plate motion beneath the Atlantic Ocean basin to the east. It is possible that lateral transitions in lithospheric anisotropy also play a role in generating QL phases, but given the peak sensitivity of 100 s surface waves to structure at depths between 100 and 200 km, it is likely that anisotropy in the asthenospheric mantle is the main source of the scattering. Our observations provide an independent constraint on the nature of upper mantle anisotropy in and around the ENAM region, and suggest that there is a unique anisotropic signature in the region between 32 and 40°N latitude, as we do not observe strong scattering from other portions of the margin. While the exact mechanism for the transitions in anisotropy suggested by our data cannot be uniquely determined, the QL observations documented in our study are numerous, robust, geographically consistent, and contain information about anisotropic structure in the upper mantle that is complementary to other types of seismic data. Future work on seismic anisotropy in and around this region of the ENAM passive margin that integrates constraints from SKS splitting, receiver-function analysis, surface wave dispersion, and QL scattering would be desirable, and should shed light on the distinctive anisotropy signature and its causative mechanisms.

Supplementary data to this article can be found online at https://doi.org/10.1016/j.tecto.2020.228321.

CRediT authorship contribution statement

Andrea Servali:Conceptualization, Methodology, Software, Formal analysis, Writing - original draft, Visualization.**Maureen D. Long**:Conceptualization, Methodology, Investigation, Data curation, Writing - original draft, Supervision, Project administration, Funding acquisition.**Jeffrey Park**:Methodology, Writing - review & editing.**Margaret H. Benoit**:Investigation, Funding acquisition.**John C. Aragon**:Software, Investigation, Data curation, Writing - review & editing.

Declaration of competing interest

The authors declare that they have no known competing financial interests or personal relationships that could have appeared to influence the work reported in this paper.

Acknowledgements

Seismic data from the USArray Transportable Array (doi: https://doi.org/10.7914/SN/TA), the U.S. National Seismic Network (doi: https://doi.org/10.7914/SN/US), the Central and Eastern U.S. Network (doi: https://doi.org/10.7914/SN/N4), and the Mid-Atlantic Geophysical Integrative Collaboration (MAGIC) experiment (doi: https://doi.org/10.7914/SN/7A_2013) were accessed via the Data Management Center (DMC; http://ds.iris.edu) of the Incorporated Research Institutions for Seismology (IRIS). The MAGIC deployment was supported by the IRIS PASSCAL Instrument Center at New Mexico Tech. The facilities of the IRIS Consortium are supported by the National Science Foundation (NSF) under Cooperative Agreement EAR-1261681 and the DOE National Nuclear Security Administration. The MAGIC project was supported by the EarthScope and GeoPRISMS programs of NSF via grant EAR-1251515 to Yale University and grant EAR-1251329 to the College of New Jersey. J. Park was supported by the EarthScope program of NSF via grant EAR-1818654. Most figures were drafted using the Generic Mapping Tools (Wessel and Smith, 1999). The NSF I/D program helped support preparation of this manuscript. Any opinion, findings, and conclusions or recommendations expressed in this article are those of the authors and do not necessarily reflect the views of the National Science Foundation. We are grateful to the editor and to two anonymous reviewers whose constructive comments helped to improve the presentation of the material.

References

Accardo, N.J., Wiens, D.A., Hernandez, S., Aster, R.C., Nyblade, A., 2014. Upper mantle seismic anisotropy beneath the West Antarctic Rift System and surrounding region from shear wave splitting analysis. Geophys. J. Int. 198, 414–429. https://doi.org/

10.1093/gji/ggu117.
Aragon, J.C., Long, M.D., Benoit, M.H., 2017. Lateral variations in SKS splitting across the MAGIC array, Central Appalachians. Geochem. Geophys. Geosyst. 18, 4136–4155. https://doi.org/10.1029/2017GC007169.
Barruol, G., Silver, P.G., Vauchez, A., 1997. Seismic anisotropy in the eastern United States: deep structure of a complex continental plate. J. Geophys. Res. – Solid Earth 102, 8329–8348. https://doi.org/10.1029/96JB038000.
Bassin, C., Laske, G., Masters, G., 2000. The current limits of resolution for surface wave tomography in North America. Eos Trans. AGU 81, F897.
Benoit, M.H., Long, M.D., King, S.D., 2013. Anomalously thin transition zone and apparently isotropic upper mantle beneath Bermuda: evidence for upwelling. Geochem. Geophys. Geosyst. 14, 4282–4291. https://doi.org/10.1002/ggge.20277.
Bishop, B.T., Beck, S.L., Zandt, G., Wagner, L., Long, M.D., Knezevic Antonijevic, S., Kumar, A., Tavera, H., 2017. Causes and consequences of flat-slab subduction in southern Peru. Geosphere 13 (doi:10.10.1130/GES0140.1).
Burton, W.C., Southworth, S., 2010. A model for Iapetan rifting of Laurentia based on Neoproterozoic dikes and related rocks. In: Tollo, R.P. (Ed.), From Rodinia to Pangea: The Lithotectonic Record of the Appalachian Region, Geological Society of America Memior. 206. pp. 45–476 10/1130/2010.1206(20).
Byrnes, J.S., Bezada, M., Long, M.D., Benoit, M.H., 2019. Thin lithosphere beneath the central Appalachian Mountains: constraints from seismic attenuation beneath the MAGIC array. Earth Planet. Sci. Lett. 519, 297–307.
Chen, X., Park, J., 2013. Anisotropy gradients from QL surface waves: evidence for vertically coherent deformation in the Tibet region. Tectonophysics 608, 346–355.
Chen, X., Li, Y., Levin, V., 2018. Shear wave splitting beneath eastern North American continent: evidence for a multilayered and laterally variable anisotropic structure. Geochem. Geophys. Geosyst. 19, 2857–2871. https://doi.org/10.1029/2018GC007646.
Darbyshire, F.A., Dahl-Jensen, T., Larsen, T.B., Voss, P.H., Joyal, G., 2018. Crust and uppermost-mantle structure of Greenland and the Northwest Atlantic from Rayleigh wave group velocity tomography. Geophys. J. Int. 212, 1546–1569.
Debayle, E., Ricard, Y., 2013. Seismic observations of large-scale deformation at the bottom of fast-moving plates. Earth Planet. Sci. Lett. 376, 165–177.
Denolle, M.A., Fan, W., Shearer, P.M., 2015. Dynamics of the 2015 M7.8 Nepal earthquake. Geophys. Res. Lett. 42. https://doi.org/10.1002/2015GL065336.
Deschamps, F., Lebedev, S., Meier, T., Trampert, J., 2008. Stratified seismic anisotropy reveals past and present deformation beneath the East-central United States. Earth Planet. Sci. Lett. 274, 489–498.
Eakin, C.M., Long, M.D., Beck, S.L., Wagner, L.S., Tavera, H., Condori, C., 2014. Response of the mantle to flat slab evolution: insights from local S splitting beneath Peru. Geophys. Res. Lett. 41, 3438–3446. https://doi.org/10.1002/2014GL059943.
Eilon, Z., Abers, G.A., Jin, G., Gaherty, J.B., 2014. Anisotropy beneath a highly extended continental rift. Geochem. Geophys. Geosyst. 15, 545–564. https://doi.org/10.1002/2013GC005092.
Ekström, G., Nettles, M., Dziewonski, A.M., 2012. The global CMT project 2004-2010: centroid-moment tensors for 13,017 earthquakes. Phys. Earth Planet. Inter. 200–201, 1–9.
Evans, R.L., Benoit, M.H., Elsenbeck, J., Long, M.D., Ford, H.A., Zhu, J., Garcia, X., 2019. Thin lithosphere beneath the central Appalachian Mountains: a combined seismic and magnetotelluric study. Earth Planet. Sci. Lett. 519, 308–316.
Fan, W., Shearer, P.M., 2015. Detailed rupture imaging of the 25 April 2015 Nepal earthquake using teleseismic P waves. Geophys. Res. Lett. 42, 5744–5752. https://doi.org/10.1002/2015GL064587.
Fischer, K.M., Ford, H.A., Abt, D.L., Rychert, C.A., 2010. The lithosphere-asthenosphere boundary. Annu. Rev. Earth Planet. Sci. 38, 551–575.
Fouch, M.J., Fischer, K.M., Parmentier, E.M., 2000. Shear wave splitting, continental keels, and patterns of mantle flow. J. Geophys. Res. 105, 6255–6275.
Frizon de Lamotte, D., Fourdan, B., Leleu, S., Leparmentier, F., de Clarens, P., 2015. Style of rifting and the stages of Pangea breakup. Tectonics 34, 1009–1029. https://doi.org/10.1002/2014TC003760.
Garzione, C.N., McQuarrie, N., Perez, N.D., Ehlers, T.A., Beck, S.L., Kar, N., Eichelberger, N., Chapman, A.D., Ward, K.M., Ducea, M.N., Lease, R.O., Poulsen, C.J., Wagner, L.S., Saylor, J.E., Zandt, G., Horton, B.K., 2017. Tectonic evolution of the Central Andean Plateau and implication for the growth of plateaus. Annu. Rev. Earth Planet. Sci. 45, 529–559.
Gashawbeza, E.M., Klemperer, S.L., Nyblade, A.A., Walker, K.T., Keranen, K.M., 2004. Shear-wave splitting in Ethiopia: Precambrian mantle anisotropy locally modified by Neogene rifting. Geophys. Res. Lett. 31, L18602. https://doi.org/10.1029/2004GL020471.
Grandin, R., Vallée, M., Satriano, C., Lacassin, R., Klinger, Y., Simoes, M., Bollinger, L., 2015. Rupture process of the Mw = 7.9 Gorkha earthquake (Nepal): insights into Himalayan megathrust segmentation. Geophys. Res. Lett. 42, 8373–8382. https://doi.org/10.1002/2015GL066044.
Hatcher Jr., R.D., 2010. The Appalachian orogeny: A brief summary. In: Tollo, R.P., Bartholomew, M.J., Hibbard, J.P., Karabinos, P.M. (Eds.), From Rodinia to Pangea: The Lithotectonic Record of the Appalachian Region. Memoir 206. Geological Society of America, Boulder, CO, pp. 1–19.
Hibbard, J.P., van Staal, C.R., Rankin, D.W., 2010. In: Tollo, R.P., Bartholomew, M.J., Hibbard, J.P., Karabinos, P.M., From Rodinia to Pangea: The Lithotectonic Record of the Appalachian Region (Eds.), Comparative analysis of the geological evolution of the northern and southern Appalachian orogeny: Late Ordovician-Permian. Geological Society of America, Boulder, CO, pp. 51–69 Memoir 206.
Huybrechts, P., 2002. Sea-level changes at the LGM from ice-dynamic reconstructions of the Greenland and Antarctic ice sheets during the glacial cycles. Quaternary Sci. Rev. 21, 203–231.
IRIS DMC, 2014. Data Services Products: Source Time Function Short-Arc Rayleigh Wave Source-Time Functions. https://doi.org/10.17611/DP/10090670.
Ji, C., Tsuboi, S., Komatitsch, D., Tromp, J., 2005. Rayleigh-wave mutipathing along the west coast of North America. Bull. Seism. Soc. Am. 95, 2115–2124. https://doi.org/10.1785/0120040180.
Kaislaniemi, L., van Hunen, J., 2014. Dynamics of lithospheric thinning and mantle melting by edge-driven convection: Application to Moroccan Atlas mountains. Geochem. Geophys. Geosyst. 15, 3175–3189. https://doi.org/10.1002/2014GC005414.
Karato, S., Jung, H., Katayama, I., Skemer, P., 2008. Geodynamic significance of seismic anisotropy of the upper mantle: new insights from laboratory studies. Annu. Rev. Earth Planet. Sci. 36, 59–95. https://doi.org/10.1146/annurev.earth.36.031207.124120.
King, S.D., 2007. Hotspots and edge-driven convection. Geology 35, 223–226. https://doi.org/10.1130/G23291A.1.
King, S.D., Anderson, D.L., 1998. Edge-driven convection. Earth Planet. Sci. Lett. 160, 289–296. https://doi.org/10.1016/S0012-821X(98)00089-2.
King, S.D., Ritsema, J., 2000. African hot spot volcanism: small-scale convection in the upper mantle beneath cratons. Science 290, 1137–1140.
Kumar, P., Kind, R., Hanka, W., Wylegalla, K., Reigber, C., Yuan, X., Woelbern, I., Schwintzer, P., Fleming, K., Dahl-Jensen, T., Larsen, T.B., Schweitzer, J., Priestley, K., Gudmundsson, O., Wolf, D., 2009. The lithosphere-asthenosphere boundary in the North-West Atlantic region. Earth Planet. Sci. Lett. 236, 249–257.
Kustowski, B., Ekström, G., Dziewoński, A.M., 2008. Anisotropic shear-wave velocity structure of the Earth's mantle: a global model. J. Geophys. Res. 113, B06306. https://doi.org/10.1029/2007JB005169.
Levin, V., Menke, W., Park, J., 1999. Shear wave splitting in the Appalachians and the Urals: a case for multilayered anisotropy. J. Geophys. Res. Solid Earth 104, 17,975–17,993. https://doi.org/10.1029/1999JB900168.
Levin, V., Park, J., Lucente, F.P., Margheriti, L., Pondrelli, S., 2007. End of subduction in northern Apennines confirmed by observations of quasi-Love waves from the great 2004 Sumatra-Andaman earthquake. Geophys. Res. Lett. 34, L04304. https://doi.org/10.1029/2006GL028860.
Levin, V., Long, M.D., Skryzalin, P., Li, Y., Lopez, I., 2018. Seismic evidence for a recently formed mantle upwelling beneath New England. Geology 46, 87–90.
Li, Z.X., Bogdanova, S.V., Collins, A.S., Davidson, A., De Waele, B., Ernst, R.E., Fitzsimons, I.C.W., Fuck, R.A., Gladkochub, D.P., Jacobs, J., Karlstrom, K.E., Lu, S., Natapov, L.M., Pease, V., Pisarevsky, S.A., Thrane, K., Vernikovsky, V., 2008. Assembly, configuration, and break-up history of Rodinia: a synthesis. Precambrian Res. 160 (1-2), 179–210.
Long, M.D., Silver, P.G., 2009. Shear wave splitting and mantle anisotropy: measurements, interpretations, and new directions. Surv. Geophys. 30, 407–461. https://doi.org/10.1007/s10712-009-9075-1.
Long, M.D., Benoit, M.H., Chapman, M.C., King, S.D., 2010. Upper mantle seismic anisotropy and transition zone thickness beneath southeastern North America and implications for mantle dynamics. Geochem. Geophy. Geosyst. 11, Q10012. https://doi.org/10.1029/2010GC003247.
Long, M.D., Till, C.B., Druken, K.A., Carlson, R.W., Wagner, L.S., Fouch, M.J., James, D.E., Grove, T.L., Schmerr, N., Kincaid, C., 2012. Mantle dynamics beneath the Pacific Northwest and the generation of voluminous back-arc volcanism. Geochem. Geophys. Geosyst. 13, Q0AN01. https://doi.org/10.1029/2012GC004189.
Long, M.D., Jackson, K.G., McNamara, J.F., 2016. *SKS* splitting beneath Transportable Array stations in eastern North America and the signature of past lithospheric deformation. Geochem. Geophys. Geosyst. 17, 2–15. https://doi.org/10.1002/2015GC006088.
Long, M.D., Benoit, M.H., Aragon, J.C., King, S.D., 2019. Seismic imaging of mid-crustal structure beneath central and eastern North America: possibly the elusive Grenville deformation? Geology 47, 371–374. https://doi.org/10.1130/G46077.1.
Lynner, C., Bodmer, M., 2017. Mantle flow along the eastern North American margin inferred from shear wave splitting. Geology 45, 867–870.
Margheriti, L., Lucente, F.P., Park, J., Pondrelli, S., Levin, V., Steckler, M., Baccheschi, P., Salimbeni, S., 2014. Large-scale coherent anisotropy of upper mantle beneath the Italian peninsula, comparing quasi-Love waves and SKS splitting. J. Geodyn. 82, 26–38. https://doi.org/10.1016/j.jog.2014.07.007.
Mazza, S.E., Gazel, E., Johnson, E.A., Kunk, M.J., McAleer, R., Spotila, J.A., Bizimis, M., Coleman, D.S., 2014. Volcanoes of the passive margin: the youngest magmatic event in eastern North America. Geology 42, 483–486. https://doi.org/10.1130/G35407.1.
Mazza, S.E., Gazel, E., Johnson, E.A., Bizimis, M., McAleer, R., Biryol, C.B., 2017. Post-rift magmatic evolution of the eastern North American "passive-aggressive" margin. Geochem. Geophys. Geosyst. 18, 3–22. https://doi.org/10.1002/2016GC006646.
Mazza, S.E., Gazel, E., Bizimis, M., Moucha, R., Béguelin, P., Johnson, E.A., McAleer, R.J., Sobolev, A.V., 2019. Sampling the volatile-rich transition zone beneath Bermuda. Nature 569, 398–403.
McHone, J.G., 1996. Broad-terrane Jurassic flood basalts across northeastern North America. Geology 24, 319–322.
McHone, J.G., 2000. Non-plume magmatism and tectonics during the opening of the Central Atlantic Ocean. Tectonophysics 316, 287–296.
McLelland, J.M., Selleck, M.W., Bickford, M.E., 2010. Review of the Proterozoic evolution of the Grenville province, its Adirondack outlier, and the Mesoproterozoic inliers of the Appalachians. In: Tollo, R.P., Bartholomew, M.J., Hibbard, J.P., Karabinos, P.M. (Eds.), From Rodinia to Pangea: The Lithotectonic Record of the Appalachian Region. Memoir 206. Geological Society of America, Boulder, CO, pp. 21–49.
Menke, W., Skryzalin, P., Levin, V., Harper, T., Darbyshire, F., Dong, T., 2016. The Northern Appalachian Anomaly: a modern asthenospheric upwelling. Geophys. Res. Lett. 43, 10,173–10,179. https://doi.org/10.1002/2016GL070918.
Menke, W., Lamoureux, J., Abbott, D., Hopper, E., Hutson, D., Marrero, A., 2018. Crustal heating and lithospheric alteration and erosion associated with asthenospheric

upwelling beneath southern New England (USA). J. Geophys. Res. Solid Earth 123, 8995–9008. https://doi.org/10.1029/2018JB015921.
Miller, S.R., Sak, P.B., Kirby, E., Bierman, P.R., 2013. Neogene rejuvenation of central Appalachian topography: evidence for differential rock uplift from stream profiles and erosion rates. Earth Planet. Sci. Lett. 369, 1–12. https://doi.org/10.1016/j.epsl.2013.04.007.
Murphy, B.S., Egbert, G.D., 2017. Electrical conductivity structure of southeastern North America: implications for lithospheric architecture and Appalachian topographic rejuvenation. Earth Planet. Sci. Lett. 462, 66–75.
Murphy, B.S., Egbert, G.D., 2019. Synthesizing seemingly contradictory seismic and magnetotelluric observations in the southeastern United States to image physical properties of the lithosphere. Geochem. Geophys. Geosyst. 20. https://doi.org/10.1029/2019GC008279.
Oda, H., Onishi, S., 2001. The effect of regional variation of lattice preferred orientation on surface waveforms. Geophys. J. Int. 144, 247–258.
Park, J., 1997. Free oscillations in an anisotropic mantle: path-integral asymptotics. Geophys. J. Int. 129, 399–411.
Park, J., Yu, Y., 1993. Seismic determination of elastic anisotropy and mantle flow. Science 261, 1159–1162.
Rieger, D.M., Park, J., 2010. USArray observations of quasi-Love surface wave scattering: orienting anisotropy in the Cascadia plate boundary. J. Geophys. Res. 115, B055306. https://doi.org/10.1029/2009JB006754.
Rivers, T., 1997. Lithotectonic elements of the Grenville province: review and tectonic implications. Precambrian Res. 86, 117–154. https://doi.org/10.1016/S0301-9268(97)00038-7.
Rivers, T., 2009. The Grenville province as a large hot long-duration collisional orogen – insights from the spatial and thermal evolution of its orogenic fronts. In: Murphy, J.B., Keppie, J.D., Hynes, A.J. (Eds.), Ancient Orogens and Modern Analogues. 327. Geological Society of London, Special Publications, pp. 405–444.
Rychert, C.A., Rondenay, S., Fischer, K.M., 2007. P-to-S and S-to-P imaging of a sharp lithosphere-asthenosphere boundary beneath eastern North America. J. Geophys. Res. 112, B08314. https://doi.org/10.1029/2006JB004619.
Savage, M.K., 1999. Seismic anisotropy and mantle deformation: what have we learned from shear wave splitting? Rev. Geophys. 37, 65–106. https://doi.org/10.1029/98RG02075.
Schlische, R.W., 2003. Progress in understanding the structural geology, basin evolution, and tectonic history of the eastern North American rift system. In: LeTorneau, P.M., Olsen, P.E. (Eds.), The Great Rift Valleys of Pangea. Columbia University Press, New York.
Schmandt, B., Lin, F.-C., 2014. P and S wave tomography of the mantle beneath the United States. Geophys. Res. Lett. 41, 6342–6349. https://doi.org/10.1002/2014GL061231.
Shuck, B., van Avendonk, H.J., 2016. Evolution of the upper lithosphere in the ENAM area from 3-D wide-angle seismic data. In: AGU Fall Meeting, Abstract T51G-2998.
Silver, P.G., 1996. Seismic anisotropy beneath the continents: probing the depths of geology. Annu. Rev. Earth Planet. Sci. 24, 385–432.
Skemer, P., Hansen, L.N., 2016. Inferring upper-mantle flow from seismic anisotropy: an experimental perspective. Tectonophysics 668–669, 1–14.
Tromp, J., Komatitsch, D., Hjörleifsdóttir, V., Liu, Q., Zhu, H., Peter, D., Bozdag, E., McRitchie, D., Friberg, P., Trabant, C., Hutko, A., 2010. Near real-time simulations of global CMT earthquakes. Geophys. J. Int. 183, 381–389.
Ucisik, N., Gudmundsson, Ó., Priestly, K., Larsen, T.B., 2005. Seismic anisotropy beneath East Greenland revealed by shear wave splitting. Geophys. Res. Lett. 32, L08315. https://doi.org/10.1029/2004GL021875.
Ucisik, N., Gudmundsson, Ó., Hanka, W., Dahl-Jensen, T., Mosegaard, K., Pristley, K., 2008. Variations of shear-wave splitting in Greenland: mantle anisotropy and possible impact of the Iceland plume. Tectonophysics 462, 137–148.
Wagner, L.S., Long, M.D., 2013. Distinctive upper mantle anisotropy beneath the High Lava Plains and Eastern Snake River Plain, Pacific Northwest, USA. Geochem. Geophys. Geosyst. 14, 4647–4666. https://doi.org/10.1002/ggge.20275.
Wagner, L.S., Long, M.D., Johnston, M.D., Benoit, M.H., 2012. Lithospheric and asthenospheric contributions to shear-wave splitting observations in the southeastern United States. Earth Planet. Sci. Lett. 341, 128–138. https://doi.org/10.1016/j.epsl.2012.06.020.
Wagner, L.S., Fisher, K.M., Hawman, R., Hopper, E., Howell, D., 2018. The relative roles of inheritance and long-term passive margin lithospheric evolution on the modern structure and tectonic activity in the southeastern United States. Geosphere 14, 1385–1410. https://doi.org/10.1130/GES01593.1.
Wessel, P., Smith, W.H.F., 1999. Free software helps map and display data. EOS Trans. Am. Geophys. Union 72, 441. https://doi.org/10.1029/90EO00319.
White-Gaynor, A.L., Nyblade, A.A., 2017. Shear wave splitting across the Mid-Atlantic region of North America: a fossil anisotropy interpretation. Geology 45, 555–558. https://doi.org/10.1130/G38794.1.
Whitmeyer, S., Karlstrom, K., 2007. Tectonic model for the Proterozoic growth of North America. Geosphere 3, 220–259. https://doi.org/10.1130/GES00055.1.
Withjack, M.O., Schlische, R.W., Olsen, P.E., 2012. Development of the passive margin of eastern North America: Mesozoic rifting, igneous activity, and breakup. In: Roberts, D.G., Bally, A.W. (Eds.), Regional Geology and Tectonics: Phanerozoic Rift Systems and Sedimentary Basins, pp. 301–335.
Yang, B.B., Liu, Y., Dahm, H., Liu, K.H., Gao, S.S., 2017. Seismic azimuthal anisotropy beneath the eastern United States and its geodynamic implications. Geophys. Res. Lett. 44, 2670–2678. https://doi.org/10.1002/2016GL071227.
Yu, Y., Park, J., Wu, F., 1995. Mantle anisotropy beneath the Tibetan Plateau: evidence from long-period surface waves. Phys. Earth Planet. Inter. 87, 231–246.
Yu, C., Zhan, Z., Hauksson, E., Cochran, E.S., 2017. Strong SH-to-Love wave scattering off the Southern California continental borderland. Geophys. Res. Lett. 44, 10,208–10,215. https://doi.org/10.1002/2017GL075213.
Zheng, T., Zhu, R., Zhao, L., Ai, Y., 2012. Intralithospheric mantle structures recorded continental subduction. J. Geophys Res. – Solid Earth 117, B03308. https://doi.org/10.1029/2011JB008873.